lecular chaperone Hsp47 is another marker of FLS in human synovial tissue. FLS expansion paralleled the activity and temporal progression of RA, and could be partially reversed by anti-TNFα therapy. Our analysis revealed that many of the cadherin 11–positive Hsp47+ FLS in the hyperplastic lining area of the diseased joints of a subset of RA patients unexpectedly contained high levels of RasGRP-4 protein. Moreover, the RasGRP-4+ lining area was significantly increased in synovial tissues from RA patients compared with those from OA patients. Although monocytes contain RasGRP-4 mRNA, this signaling protein and its transcript decrease in amount when these immature progenitors differentiate into mature macrophages or osteoclasts. As expected, very few CD14+CD68+ macrophages in the arthritic synovium contained detectable amounts of RasGRP-4 protein.

Normal fibroblasts do not express RasGRP-4. Indeed, recombinant mouse and human RasGRP-4 were initially generated in transfected RasGRP-4$^{-/-}$ mouse 3T3 fibroblasts to evaluate their ability to activate Ras (15). Fibroblasts are particularly abundant in human skin, and none of the 210,759 human skin–derived ESTs in the current GenBank EST database originated from the human RasGRP-4 gene (see GenBank Hs130434; http://www.ncbi.nlm.nih.gov/UniGene/clust.cgi?UGID=148804&TAXID=9606&SEARCH=). Thus, the finding that the majority of the RasGRP-4+ cells in synovial tissue from our RA patients were FLS was unanticipated.

The levels of RasGRP-4 transcript in the FLS of some of our RA patients were considerably higher than those in every OA patient. The levels of RasGRP-4 transcript in FLS stimulated with TNFα also were significantly higher than the levels in untreated control cells, and the rate of proliferation of cultured FLS was significantly increased when these mesenchymal cells encountered TNFα. This finding might be one of the reasons why FLS from those RA patients who had been previously treated with a TNFα inhibitor tended to express less RasGRP-4.

The abnormally high rate of proliferation of FLS at the synovial intimal lining layer is a prominent feature of RA. The correlation between the levels of RasGRP-4 transcript and the proliferation rate of FLS supports the importance of TNFα and the downstream signaling protein RasGRP-4 in unchecked growth of FLS in the joints of some patients with RA. The MAPK cascade, which is stimulated by engagement of cytokine and Toll-like receptors, is the most extensively studied pathway in FLS. MAPK signaling involves the activation of 3 levels of kinases. The top tier includes MAPKK kinase. The middle level includes MAPK kinase, and the distal level comprises ERK, p38 MAPKs, and JNK (40). ERK-1/2 is also important in MMP-1– and cyclooxygenase 2 (COX-2)–dependent prostaglandin E_2 (PGE_2) generation in FLS (41,42). ERK-1/2 signaling has been implicated in the chronic aspects of RA (40). Because RasGRP-4 is a GEF that activates Ras (15), it therefore was not surprising that the levels of its transcript were correlated with the proliferation potency of FLS.

FLS from a subset of RA patients decreased their proliferation when exposed to a RasGRP-4–specific siRNA. FLS express RANKL, IL-6, VEGF, MMP-1, MMP-3, and mPGES (38). Although levels of transcripts that encode RANKL, IL-6, VEGF, and MMP-3 were unaltered in FLS that had been exposed to RasGRP-4–specific siRNA, levels of MMP-1 and mPGES-1 transcripts were significantly decreased in these cells. MMP-1 is a neutral protease expressed by stromal cells, and it participates in the destruction of cartilage and remodeling of its damaged extracellular matrix (41). Microsomal PGES is an enzyme that acts downstream of COX-2; it catalyzes the final step of PGE_2 biosynthesis. Proinflammatory cytokine–activated cells (e.g., synovial cells, chondrocytes, and macrophages) are the primary sources of PGE_2 in the inflamed joints of RA patients. COX-2 has been targeted for the treatment of RA by using NSAIDs, including selective COX-2 inhibitors (39).

We showed that rats with CIA that had received an intraarticular injection of a RasGRP-4–specific siRNA had significantly improved arthritis and scarce joint destruction, consistent with the recent finding that RasGRP-4–null B6 mice are resistant to experimental K/BxN arthritis (27). Thus, the importance of RasGRP-4 in a second well-established experimental arthritis model has now been shown.

In the present study, we demonstrated that inhibition of RasGRP-4 resulted in reduced proliferation of FLS in vitro and in diminished arthritis and joint destruction in a rat disease model. Thus, RasGRP-4 is an attractive treatment target in RA patients.

ACKNOWLEDGMENTS

The authors acknowledge Drs. Tsutomu Endo and Masahiko Takahata for providing synovial tissue and assisting with micro-CT. We also thank Dr. Akihiro Ishizu for technical support and valuable discussion.

AUTHOR CONTRIBUTIONS

All authors were involved in drafting the article or revising it critically for important intellectual content, and all authors approved the final version to be published. Dr. Yasuda had full access to all of the data in the study and takes responsibility for the integrity of the data and the accuracy of the data analysis.

Study conception and design. Kono, Yasuda, Stevens.

Acquisition of data. Kono, Yasuda, Koide, Y. Shimizu, T. Shimizu, Majima.

Analysis and interpretation of data. Kono, Yasuda, Stevens, Kurita, Kanetsuka, Oku, Bohgaki, Amengual, Horita, Koike, Atsumi.

REFERENCES

1. McInnes IB, Schett G. The pathogenesis of rheumatoid arthritis. N Engl J Med 2011;365:2205–19.
2. Smolen JS, Breedveld FC, Schiff MH, Kalden JR, Emery P, Eberl G, et al. A Simplified Disease Activity Index for rheumatoid arthritis for use in clinical practice. Rheumatology (Oxford) 2003;42:244–57.
3. Scott DL, Wolfe F, Huizinga TW. Rheumatoid arthritis. Lancet 2010;376:1094–108.
4. Felson DT, Smolen JS, Wells G, Zhang B, van Tuyl LH, Funovits J, et al. American College of Rheumatology/European League Against Rheumatism provisional definition of remission in rheumatoid arthritis for clinical trials. Arthritis Rheum 2011;63: 573–86.
5. Bartok B, Firestein GS. Fibroblast-like synoviocytes: key effector cells in rheumatoid arthritis. Immunol Rev 2010;233:233–55.
6. Lee A, Qiao Y, Grigoriev G, Chen J, Park-Min KH, Park SH, et al. Tumor necrosis factor α induces sustained signaling and a prolonged and unremitting inflammatory response in rheumatoid arthritis synovial fibroblasts. Arthritis Rheum 2013;65:928–38.
7. Hascall VC, Sajdera SW. Proteinpolysaccharide complex from bovine nasal cartilage: the function of glycoprotein in the formation of aggregates. J Biol Chem 1969;244:2384–96.
8. Gotis-Graham I, Smith MD, Parker A, McNeil HP. Synovial mast cell responses during clinical improvement in early rheumatoid arthritis. Ann Rheum Dis 1998;57:664–71.
9. Gruber B, Poznansky M, Boss E, Partin J, Gorevic P, Kaplan AP. Characterization and functional studies of rheumatoid synovial mast cells: activation by secretagogues, anti-IgE, and a histamine-releasing lymphokine. Arthritis Rheum 1986;29:944–55.
10. Nigrovic PA, Lee DM. Synovial mast cells: role in acute and chronic arthritis. Immunol Rev 2007;217:19–37.
11. Van den Broek MF, van den Berg WB, van de Putte LB. The role of mast cells in antigen induced arthritis in mice. J Rheumatol 1988;15:544–51.
12. Lee DM, Friend DS, Gurish MF, Benoist C, Mathis D, Brenner MB. Mast cells: a cellular link between autoantibodies and inflammatory arthritis. Science 2002;297:1689–92.
13. McNeil HP, Shin K, Campbell IK, Wicks IP, Adachi R, Lee DM, et al. The mouse mast cell–restricted tetramer-forming tryptases mouse mast cell protease 6 and mouse mast cell protease 7 are critical mediators in inflammatory arthritis. Arthritis Rheum 2008; 58:2338–46.
14. Shin K, Nigrovic PA, Crish J, Boilard E, McNeil HP, Larabee KS, et al. Mast cells contribute to autoimmune inflammatory arthritis via their tryptase/heparin complexes. J Immunol 2009;182:647–56.
15. Yang Y, Li L, Wong GW, Krilis SA, Madhusudhan MS, Sali A, et al. RasGRP4, a new mast cell-restricted Ras guanine nucleotide-releasing protein with calcium- and diacylglycerol-binding motifs: identification of defective variants of this signaling protein in asthma, mastocytosis, and mast cell leukemia patients and demonstration of the importance of RasGRP4 in mast cell development and function. J Biol Chem 2002;277:25756–74.
16. Li L, Yang Y, Stevens RL. Cloning of rat Ras guanine nucleotide releasing protein 4, and evaluation of its expression in rat mast cells and their bone marrow progenitors. Mol Immunol 2002;38: 1283–8.
17. Li L, Yang Y, Wong GW, Stevens RL. Mast cells in airway hyporesponsive C3H/HeJ mice express a unique isoform of the signaling protein Ras guanine nucleotide releasing protein 4 that is unresponsive to diacylglycerol and phorbol esters. J Immunol 2003;171:390–7.
18. Hashimoto T, Yasuda S, Koide H, Kataoka H, Horita T, Atsumi T, et al. Aberrant splicing of the hRasGRP4 transcript and decreased levels of this signaling protein in the peripheral blood mononuclear cells in a subset of patients with rheumatoid arthritis. Arthritis Res Ther 2011;13:R154.
19. Suire S, Lecureuil C, Anderson KE, Damoulakis G, Niewczas I, Davidson K, et al. GPCR activation of Ras and PI3Kc in neutrophils depends on PLCb2/b3 and the RasGEF RasGRP4. EMBO J 2012;31:3118–29.
20. Reuther GW, Lambert QT, Rebhun JF, Caligiuri MA, Quilliam LA, Der CJ. RasGRP4 is a novel Ras activator isolated from acute myeloid leukemia. J Biol Chem 2002;277:30508–14.
21. Ebinu JO, Bottorff DA, Chan EY, Stang SL, Dunn RJ, Stone JC. RasGRP, a Ras guanyl nucleotide-releasing protein with calcium- and diacylglycerol-binding motifs. Science 1998;280:1082–6.
22. Tognon CE, Kirk HE, Passmore LA, Whitehead IP, Der CJ, Kay RJ. Regulation of RasGRP via a phorbol ester-responsive C1 domain. Mol Cell Biol 1998;18:6995–7008.
23. Clyde-Smith J, Silins G, Gartside M, Grimmond S, Etheridge M, Apolloni A, et al. Characterization of RasGRP2, a plasma membrane-targeted, dual specificity Ras/Rap exchange factor. J Biol Chem 2000;275:32260–7.
24. Yamashita S, Mochizuki N, Ohba Y, Tobiume M, Okada Y, Sawa H, et al. CalDAG-GEFIII activation of Ras, R-ras, and Rap1. J Biol Chem 2000;275:25488–93.
25. Li J, Shen H, Himmel KL, Dupuy AJ, Largaespada DA, Nakamura T, et al. Leukaemia disease genes: large-scale cloning and pathway predictions. Nat Genet 1999;23:348–53.
26. Suzuki T, Shen H, Akagi K, Morse HC, Malley JD, Naiman DQ, et al. New genes involved in cancer identified by retroviral tagging. Nat Genet 2002;32:166–74.
27. Adachi R, Krilis SA, Nigrovic PA, Hamilton MJ, Chung K, Thakurdas SM, et al. Ras guanine nucleotide-releasing protein-4 (RasGRP4) involvement in experimental arthritis and colitis. J Biol Chem 2012;287:20047–55.
28. Aletaha D, Neogi T, Silman AJ, Funovits J, Felson DT, Bingham CO III, et al. 2010 rheumatoid arthritis classification criteria: an American College of Rheumatology/European League Against Rheumatism collaborative initiative. Arthritis Rheum 2010;62: 2569–81.
29. Fukae J, Amasaki Y, Yamashita Y, Bohgaki T, Yasuda S, Jodo S, et al. Butyrate suppresses tumor necrosis factor α production by regulating specific messenger RNA degradation mediated through a cis-acting AU-rich element. Arthritis Rheum 2005;52:2697–707.
30. Izquierdo E, Canete JD, Celis R, Del Rey MJ, Usategui A, Marsal S, et al. Synovial fibroblast hyperplasia in rheumatoid arthritis: clinicopathologic correlations and partial reversal by anti–tumor necrosis factor therapy. Arthritis Rheum 2011;63:2575–83.
31. Earp JC, Dubois DC, Molano DS, Pyszczynski NA, Keller CE, Almon RR, et al. Modeling corticosteroid effects in a rat model of rheumatoid arthritis. I. Mechanistic disease progression model for the time course of collagen-induced arthritis in Lewis rats. J Pharmacol Exp Ther 2008;326:532–45.
32. Minakuchi Y, Takeshita F, Kosaka N, Sasaki H, Yamamoto Y, Kouno M, et al. Atelocollagen-mediated synthetic small interfer-

ing RNA delivery for effective gene silencing in vitro and in vivo. Nucleic Acids Res 2004;32:e109.
33. Siebuhr AS, Wang J, Karsdal M, Bay-Jensen AC, Jin Y, Zheng Q. Matrix metalloproteinase-dependent turnover of cartilage, synovial membrane, and connective tissue is elevated in rats with collagen induced arthritis. J Transl Med 2012;10:195.
34. Pine PR, Chang B, Schoettler N, Banquerigo ML, Wang S, Lau A, et al. Inflammation and bone erosion are suppressed in models of rheumatoid arthritis following treatment with a novel Syk inhibitor. Clin Immunol 2007;124:244–57.
35. Coppieters K, Dreier T, Silence K, de Haard H, Lauwereys M, Casteels P, et al. Formatted anti–tumor necrosis factor α VHH proteins derived from camelids show superior potency and targeting to inflamed joints in a murine model of collagen-induced arthritis. Arthritis Rheum 2006;54:1856–66.
36. Lee DM, Kiener HP, Agarwal SK, Noss EH, Watts GF, Chisaka O, et al. Cadherin-11 in synovial lining formation and pathology in arthritis. Science 2007;315:1006–10.
37. Huber LC, Distler O, Tarner I, Gay RE, Gay S, Pap T. Synovial fibroblasts: key players in rheumatoid arthritis. Rheumatology (Oxford) 2006;45:669–75.
38. Bottini N, Firestein GS. Duality of fibroblast-like synoviocytes in RA: passive responders and imprinted aggressors. Nat Rev Rheumatol 2013;9:24–33.
39. Kojima F, Matnani RG, Kawai S, Ushikubi F, Crofford LJ. Potential roles of microsomal prostaglandin E synthase-1 in rheumatoid arthritis. Inflamm Regen 2011;31:157–66.
40. Paunovic V, Harnett MM. Mitogen-activated protein kinases as therapeutic targets for rheumatoid arthritis. Drugs 2013;73: 101–15.
41. Barchowsky A, Frleta D, Vincenti MP. Integration of the NF-κB and mitogen-activated protein kinase/AP-1 pathways at the collagenase-1 promoter: divergence of IL-1 and TNF-dependent signal transduction in rabbit primary synovial fibroblasts. Cytokine 2000; 12:1469–79.
42. Nah SS, Won HJ, Ha E, Kang I, Cho HY, Hur SJ, et al. Epidermal growth factor increases prostaglandin E_2 production via ERK1/2 MAPK and NF-κB pathway in fibroblast like synoviocytes from patients with rheumatoid arthritis. Rheumatol Int 2010;30:443–9.

Japan College of Rheumatology
MODERN RHEUMATOLOGY

http://informahealthcare.com/mor
ISSN 1439-7595 (print), 1439-7609 (online)

Mod Rheumatol, 2014; Early Online: 1–8
© 2014 Japan College of Rheumatology
DOI: 10.3109/14397595.2014.950035

informa
healthcare

ORIGINAL ARTICLE

IL-6 signal blockade ameliorates the enhanced osteoclastogenesis and the associated joint destruction in a novel FcγRIIB-deficient rheumatoid arthritis mouse model

Mareki Ohtsuji[1,2], Qingshun Lin[2], Keiko Nishikawa[2], Naomi Ohtsuji[2], Hideki Okazaki[2,3], Hiromichi Tsurui[2], Hirofumi Amano[4], Toshikazu Shirai[2], Norihiro Nishimoto[5], Hiroyuki Nishimura[1], and Sachiko Hirose[2]

[1]*Department of Biomedical Engineering, Toin Human Science and Technology Center, Toin University of Yokohama, Yokohama, Japan,* [2]*Department of Pathology, Juntendo University School of Medicine, Tokyo, Japan,* [3]*Health and Life Science, Musashigaoka Junior College, Saitama, Japan,* [4]*Department of Rheumatology and Internal Medicine, Juntendo University School of Medicine, Tokyo, Japan, and* [5]*Osaka Rheumatology Clinic, Osaka, Japan*

Abstract

Objective. We earlier found that TNFα but not interleukin (IL)-17 is indispensable in the pathogenesis of spontaneously occurring rheumatoid arthritis (RA)-like disease in our newly established FcγRIIB-deficient C57BL/6 (B6) mouse model, designated KO1. Here, we examined the role of IL-6 in the pathogenesis of RA features in KO1, with particular reference to cartilage and bone destruction in arthritic joints.

Methods. To evaluate the preventive effect of MR16-1, a rat anti-mouse IL-6 receptor (IL-6R) mAb, 4-month-old preclinical KO1 mice were divided into three groups: the first treated with MR16-1 for 6 months, the second treated with normal rat IgG, as a control, and the third left untreated. The incidence and severity of arthritis, immunological abnormalities, and transcription levels of receptor activator of NF-κB ligand (RANKL), osteoprotegerin (OPG), and inflammatory cytokines/chemokines in ankle joint tissues were compared among the three groups. The therapeutic effect of MR16-1 was examined by treating 7-month-old KO1 mice in the early stages of arthritis for 2 months.

Results. Compared with the findings in the KO1 mice left untreated or treated with normal rat IgG, the development of arthritis was markedly suppressed in mice with MR16-1 treatment started from preclinical stages. The suppression was associated with the decrease in production of autoantibodies, rheumatoid factors (RF), and anti-cyclic citrullinated peptide (CCP). Histologically, marked synovitis, pannus formation, and cartilage and bone destruction associated with the increase in tartrate-resistant acid phosphatase (TRAP)-positive osteoclast generation were evident in the two control groups; however, these findings were virtually absent in MR16-1-treated mice. Real-time PCR analysis revealed that the up-regulated expression levels of MCP-1, IL-6, and TNFα, and the aberrantly high RANKL/OPG expression ratio in synovial joint tissues from the two control groups of mice with overt arthritis were significantly suppressed in MR16-1-treated mice. In mice with therapeutic MR16-1 treatment, there was no progression in arthritis score and the RANKL/OPG ratio in joint tissues was significantly suppressed.

Conclusions. Administration of an anti-IL-6R mAb ameliorated spontaneously occurring RA-like disease features, indicating that IL-6, as well as TNFα, plays a pivotal role in the pathogenesis of RA in KO1 mice. Current studies showed that, in addition to the role in enhancing autoantibody production, IL-6 promotes synovial tissue inflammation and osteoclastogenesis, leading to the severe synovitis with pannus formation and the progressive cartilage and bone destruction in multiple joints.

Keywords

Interleukin-6, MCP-1, OPG, Osteoclastogenesis, RANKL

History

Received 26 March 2014
Accepted 27 July 2014
Published online 27 August 2014

Introduction

Rheumatoid arthritis (RA) is a chronic systemic autoimmune disease, characterized by the development of synovial tissue inflammation in multiple joints followed by synovial hyperplasia with pannus formation and the progressive destruction of cartilage and bone mediated by enhanced proliferation of activated osteoclasts. The process of osteoclastogenesis is controlled by the interaction of receptor activator of NF-κB (RANK) expressed on osteoclast precursors with its ligand RANKL expressed on synovial fibroblasts, osteoblasts, and Th17 cells [1,2]. RANKL-mediated osteoclastogenesis is counterbalanced by the physiologically expressed decoy receptor, osteoprotegerin (OPG) [3]. Accumulating evidence has indicated that high expression levels of proinflammatory cytokines such as tumor necrosis factor α (TNFα), interleukin (IL)-1, IL-6, and IL-17 in inflamed synovial tissues may play a pivotal role in the processes of both synovial hyperplasia and osteoclastogenesis [4].

Correspondence to: Sachiko Hirose, MD, PhD, Department of Pathology, Juntendo University School of Medicine, 2-1-1 Hongo, Bunkyo-ku, Tokyo 113-8421, Japan. Tel: + 81-3-5802-1671. Fax: + 81-3-3813-3164. E-mail address: sacchi@juntendo.ac.jp

RIGHTSLINK

To evaluate the therapeutic potentials of targeting the proinflammatory cytokines for RA, extensive clinical studies of RA patients have been carried out by the administration of either inhibitory antibodies or antagonistic proteins. Clinical trials done by blocking the TNFα signal using anti-TNFα antibodies or TNF receptor-IgG Fc fusion protein as well as by blocking IL-1 signal using recombinant IL-1 receptor antagonist (IL-1Ra) showed that, while all these therapeutic approaches have been on the whole successful, the effects of treatments were variable and not always satisfactory for all patients [5–7]. The same was true in phase II clinical studies of RA patients under anti-IL-17 antibody administration [8].

Using several kinds of murine RA model, such cytokine blocking approaches have been carried out; however, the therapeutic effects varied considerably, depending on the RA mouse models examined. For instance, although the anti-TNFα antibody therapy was effective in the type II collagen-induced arthritis (CIA) of DBA mice [9,10], severe CIA still developed in TNFα-deficient C57BL/6 (B6) mice [11]. In the K/BxN serum transfer arthritis model, there was no evidence of any particular requirement of TNFα for bone destruction [12]. As for the role of IL-17, genetic IL-17 deficiency was reported to suppress completely the arthritis spontaneously occurring in ZAP-70-mutant SKG mice [13] and in IL-1Ra-deficient mice [14]. However, the lack of IL-17 was not fully sufficient to prevent CIA [15], and had no effect on the human cartilage proteoglycan-induced arthritis [16]. These observations, taken collectively, clearly indicate that different mechanisms underlie the pathogenesis of RA in individual patients as well as in individual mouse models; thus, further studies using several kinds of arthritis model are valuable to clarify the therapeutic mechanisms of each cytokine inhibitor for RA.

Recently, as the second-generation anti-cytokine approach, the therapeutic effects of IL-6 signal blockade using anti-IL-6 receptor (IL-6R) antibodies in RA patients were examined. A series of clinical trials have demonstrated an excellent efficacy of tocilizumab, a humanized anti-human IL-6R mAb, in trial designs either with or without methotrexate, an anchor drug for RA therapy [17–19], showing that anti-IL-6R antibodies would be an additional promising therapeutic option for RA patients. Studies in CIA mouse model likewise revealed that the treatment with anti-mouse IL-6R mAb, MR16-1, was effective to ameliorate arthritis [20]. However, both the K/BxN serum transfer arthritis and the anti-type II collagen mAb-induced arthritis normally developed in mice with genetic deficiency of IL-6 [12,21]. Thus, studies using additional arthritis mouse models are helpful to clarify the mechanism of the effect of IL-6 signal blockade on arthritis.

We recently found that a B6 mouse strain genetically deficient in inhibitory IgG Fc receptor IIB (FcγRIIB), designated KO1, spontaneously develops human RA-like disease features with marked synovial hyperplasia and severe cartilage and bone destruction in multiple joints [22]. To evaluate the role of TNFα and IL-17 in the pathogenesis of this arthritis, we earlier introduced genetic deficiency of TNFα and IL-17 in the KO1 mouse strain [23]. The results showed that TNFα-deficient KO1 mice did not develop arthritis at all; however, IL-17-deficient KO1 mice developed severe arthritis with comparable incidence and severity as those found in KO1 mice [23].

In the present studies, we treated KO1 mice with MR16-1 in order to clarify the role of IL-6 in the pathogenesis of RA-like disease in KO1 mice. Our studies revealed that the MR16-1 treatment suppressed not only RA-related autoantibody production but also RANKL-mediated osteoclastogenesis through normalizing the RANKL/OPG ratio, indicating that IL-6, as well as TNFα, plays a pivotal role in the pathogenesis of RA in this model mouse strain.

Materials and methods

Mice

Arthritis-prone KO1 is an FcγRIIB-deficient B6 congenic line [22], obtained by backcrossing the originally constructed FcγRIIB-deficient mice on a hybrid (129 × B6) background [24] into a B6 background for over 12 generations. Only female mice were analyzed in the present study. All mice were housed under identical specific-pathogen-free conditions, and all experiments were performed in accordance with our institutional guidelines.

Scoring of arthritis

Ankle joint swelling was examined by inspection and arbitrarily scored as follows: 0, no swelling; 1, mild swelling; 2, moderate swelling; and 3, severe swelling. Scores for both ankle joints were summed for each mouse, and mice with a score of 2 or over were considered positive for arthritis.

In vivo administration of anti-IL-6R mAb

To examine the preventive effect of neutralizing mAb against IL-6R on the development of RA, 4-month-old preclinical KO1 mice were randomly divided into three groups. Each group of 15 mice was left untreated, treated with normal rat IgG (Sigma Chemical Co.), or treated with rat anti-mouse IL-6R mAb (MR16-1, rat IgG1, a kind gift from Chugai Pharmaceutical, Tokyo, Japan) [25]. Two hundred micrograms of rat IgG or MR16-1 were administered i.p. twice a week for 6 months. To evaluate the therapeutic effect of MR16-1 treatment, 7-month-old mice in the early stages of arthritis with a score 1 or 2 were selected and injected i.p. with 200 μg of MR16-1 twice a week for 2 months.

Histopathology

Joint tissues were decalcified in 10% EDTA in 0.1 M Tris buffer (pH 7.4), fixed in 4% paraformaldehyde, and embedded in paraffin. Tissue sections were stained with hematoxylin/eosin, and also stained for tartrate-resistant acid phosphatase (TRAP) using the TRAP/ALP stain kit (Wako Pure Chemical Industries Ltd.).

Serum levels of antibodies

Serum levels of IgG class anti-cyclic citrullinated peptide (CCP) antibodies were measured employing commercially available kits (Cosmic Corporation) using anti-mouse IgG second antibodies and are expressed as relative units according to the manufacturer's instructions. Serum levels of rheumatoid factor (RF) were measured using an ELISA, as previously described [26]. Briefly, an ELISA plate pre-coated with mouse IgG Fc fragment (OEM Concepts) was incubated with appropriately diluted mouse serum samples, washed, and then incubated with peroxidase-conjugated rat anti-mouse κ chain antibodies (BD Biosciences Pharmingen). Activities for RF are expressed in units referring to a standard curve obtained by serial dilution of a standard serum pool from 4 to 6-month-old MRL/*lpr* mice containing 1000 unit activities/ml. Serum levels of IgG class anti-double-stranded (ds) DNA were measured using an ELISA plate pre-coated with 5 μg/ml calf thymus dsDNA (Sigma–Aldrich). DNA-binding activities are expressed in units, as previously described [22].

Flow cytometric analysis

Spleen cells were four-color-stained with the following mAbs: anti-B220, anti-CD69, anti-CD138, anti-CD3, anti-CD4, anti-CD8, and anti-CD25, and with peanut agglutinin (PNA). Foxp3 staining was performed using Foxp3/transcription Factor Staining buffer set (eBioscience). For peripheral monocyte staining,

For personal use only.

RIGHTSLINK

peripheral leukocytes were stained with anti-CD11b mAb. Stained cells were analyzed using a FACSAria cytometer and FlowJo software (Tree Star, Inc., Ashland, OR), excluding dead cells in forward and side scatter cytogram.

For intracellular cytokine staining, spleen cells were stimulated with PMA (0.2 μg/ml)/ionomycin (2 μg/ml) in the presence of Golgi-Stop (BD Bioscience) for 5 h and stained with 7-ADD (eBioscience) (staining for dead cells) and with Pacific Blue-labeled anti-CD4 mAb. Stained cells were then fixed and permeabilized using BD Cytofix/Cytoperm (BD Bioscience), followed by staining with FITC-labeled anti-TNFα and anti-IFNγ mAbs, and PE-labeled anti-IL-4 and anti-IL-7 mAbs. Stained cells were analyzed as above, excluding 7-ADD-positive cells.

Quantitative real-time PCR (qRT-PCR) analysis

Total RNA was isolated from ankle joint tissues using QIAGEN RNeasy Lipid Tissue Minikit (Cat. No. 74804). Briefly, ~25 mg of ankle joint tissue was added in 500 μl of QIAzol lysis reagent in a 2-ml tube containing 5-mm-diameter zirconia beads (Hirasawa YTZ-5) and homogenized on TissueLyser (Qiagen) for 1 min at 30 Hz. Total RNA was extracted from homogenized materials using Minikit according to the manufacturer's instructions, and the single-stranded cDNA was synthesized using an oligo(dT)-primer with Superscript II First-Strand Synthesis kit (Invitrogen). The cDNA product was used for qRT-PCR. The data were normalized to β-actin as a reference. The primer pairs used were as follows: RANKL (forward) 5′-TGTACTTTCGAGCGCAGATG-3′, (reverse) 5′-AGGCTTGTTTCATCCTCCTG-3′; OPG (forward) 5′-TGAGTGTGAGGAAGGGCGTTA-3′, (reverse) 5′-CCATC TGGACATTTTTTGCAAA-3′; MCP-1 (forward) 5′-AGGTCCC TGTCATGCTTCTG-3′, (reverse) 5′-TCTGGACCCATTCCTT CTTG-3′; RANTES (forward) 5′-TCGTGCCCACGTCAAGG AGTATTT-3′, (reverse) 5′-TCTTCTCTGGGTTGGCACACAC TT-3′; CX3CL1 (forward) 5′-CGCGTTCTTCCATTTGTGTA-3′, (reverse) 5′-CTGTGTCGTCTCCAGGACAA-3′; IL-6 (forward) 5′-GAGGATACCACTCCCAACAGACC-3′, (reverse) 5′-AAG TGCATCATCGTTGTTCATACA-3′; TNFα (forward) 5′-TAT GGCCCAGACCCTCAC-3′, (reverse) 5′-GGTTGTCTTTGAGA TCCATGC-3′; IFNγ (forward) 5′-AAGACAATCAGGCCATC AGC-3′, (reverse) 5′-ATCAGCAGCGACTCCTTTTC-3′; IL-17 (forward) 5′-TCTCTGATGCTGTTGCTGCT-3′, (reverse) 5′-GA CCAGGATCTCTTGCTGGA-3′; Foxp3 (forward) 5′-TCCTTCC CAGAGTTCTTCCA-3′, (reverse) 5′-AGGGATTGGAGCACTT GTTG-3′; RORγt (forward) 5′-GCCCTGTGTTTTTCTGAG GA-3′, (reverse) 5′-AGGGGATTCAACATCAGTGC-3′; and β-actin (forward) 5′-TGGGTATGGAATCCTGTGG-3′, (reverse) 5′-GTACTTGCGCTCAGGAGGAG-3′. The quantity was normalized using the $2^{-\Delta\Delta CT}$ method. Values of B6 mice were designated as 1, and values of each group of mice were evaluated as fold change compared with the values in B6 mice.

Statistics

Statistical analysis was carried out using the Kaplan–Meier method for the incidence of arthritis, Mann–Whitney's *U* test for antibody levels and qRT-PCR analysis, and Student's *t*-test for arthritis score and flow cytometric analysis. A value of $P < 0.05$ was considered as statistically significant.

Results

Preventive effect of MR16-1 treatment on incidence and severity of arthritis

Four-month-old disease-free KO1 mice were divided into three groups, namely untreated, normal rat IgG-treated, and MR16-1-treated groups. Figure 1a compares the cumulative incidence and severity of arthritis in ankle joints among these three groups of mice. Untreated KO1 mice spontaneously developed arthritis with swelling and limited mobility of the ankle joints symmetrically after 5 months of age, and the severity of arthritis increased with age. KO1 mice treated with normal rat IgG developed severe arthritis with comparable incidence and severity to that observed in the untreated KO1 mice. In contrast, the arthritis was markedly suppressed in MR16-1-treated KO1 mice and its incidence was only 13%, even by 10 months of age. Figure 1b shows representative macroscopic findings of hind paws of the three groups of mice at 10 months of age. Histological examination revealed severe synovitis with remarkable pannus formation and destruction of cartilage and bone in untreated KO1 and normal rat IgG-treated KO1 mice (Figure 1c upper panel). TRAP staining showed an increase in the number of TRAP-positive osteoclasts at the resorption lacuna on the surface of cartilage and bone in untreated KO1 and normal rat IgG-treated KO1 mice (Figure 1c lower panel). These changes were virtually absent in MR16-1-treated KO1 mice.

Effect on serum autoantibody levels, activation status of lymphocytes, and peripheral monocyte frequencies

Figure 2 compares the serum levels of RF and IgG class autoantibodies against CCP and dsDNA among untreated, normal rat

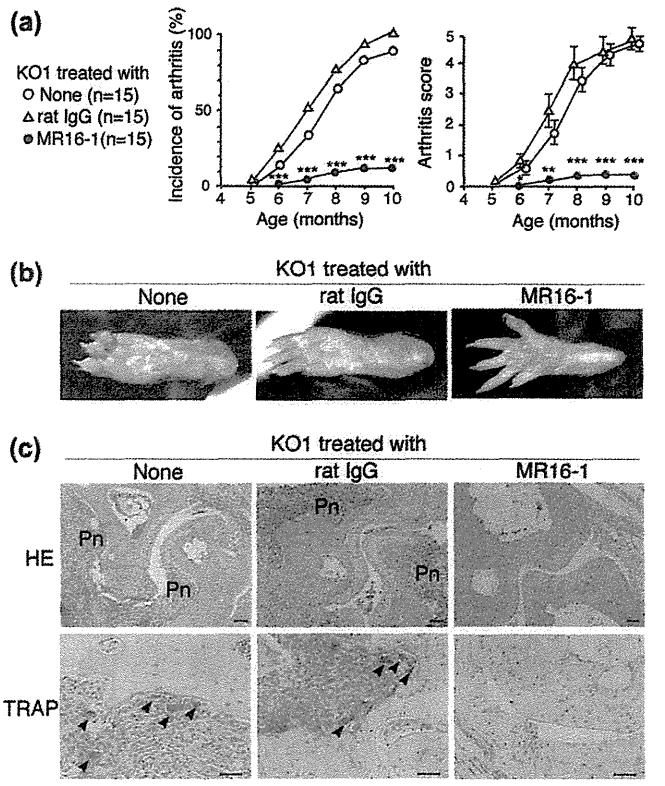

Figure 1. Preventive effect of MR16-1 treatment. (a) The cumulative incidence of arthritis and arthritis score (mean and SEM) in untreated ($n = 15$), normal rat IgG-treated ($n = 15$), and MR16-1-treated KO1 ($n = 15$) mice. Statistical significance is shown (* $P < 0.05$, ** $P < 0.01$, *** $P < 0.001$). (b) Representative macroscopic findings of hind paws in untreated, normal rat IgG-treated, and MR16-1-treated KO1 mice at 10 months of age. (c) Representative histopathological changes in finger joints in the three groups of KO1 mice at 10 months of age. Untreated and normal rat IgG-treated KO1 mice show marked synovitis with inflammatory cell infiltration, pannus formation (Pn), TRAP-positive osteoclast generation (arrowhead), and the destruction of cartilages and bones. There are no such changes in MR16-1-treated KO1 mice. Representative results obtained from six female mice in each group. Hematoxylin/eosin and TRAP staining. Bars = 50 μm.

RIGHTSLINK

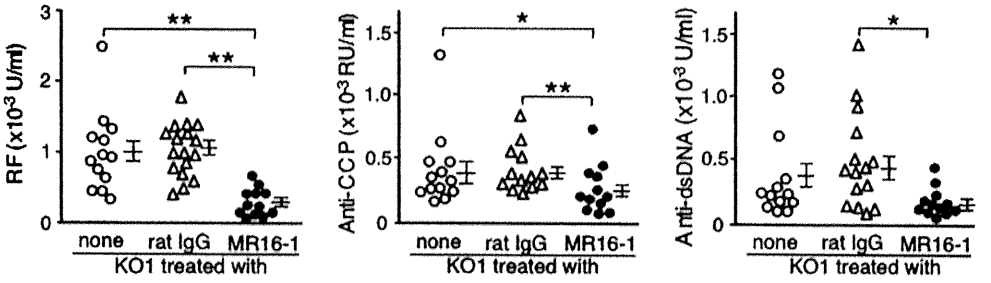

Figure 2. Comparisons of serum levels of RF, and IgG class autoantibodies against CCP and dsDNA among untreated, normal rat IgG-treated, and MR16-1-treated KO1 mice at 8 months of age. The levels of individual mice were plotted with mean and SEM. Statistical significance is shown (* $P<0.05$, ** $P<0.01$).

IgG-treated, and MR16-1-treated groups of mice at 8 months of age. Levels of RF and anti-CCP antibodies were significantly suppressed in MR16-1-treated KO1 mice compared with those in untreated and normal rat IgG-treated KO1 mice. Levels of anti-dsDNA antibodies in MR16-1-treated KO1 mice were also significantly suppressed compared with those in normal rat IgG-treated KO1 mice.

We then examined the spleen weight and the frequencies of splenic lymphocyte subsets and peripheral monocytes in mice at 9~10 months of age. As shown in Table 1, while there was no difference in the spleen weight, the frequencies of total B cells, PNA$^+$ germinal center B cells, CD138$^+$ plasma cells, CD3$^+$ T cells, and CD8$^+$ T cells among the three groups of mice, the frequencies of CD69$^+$ activated B cells per total B cells and CD4$^+$ T cells per total cells were significantly decreased in MR16-1-treated KO1 mice compared with those in untreated and normal rat IgG-treated KO1 mice. Among CD4$^+$ T cells, the frequency of CD25$^+$Foxp3$^+$ T regulatory (Treg) cells did not differ significantly among the three groups of mice. We also examined the frequencies of peripheral monocytes, which contain osteoclast precursors [27]. Compared with normal B6 mice with monocyte frequencies under 10% [28], the markedly high frequencies of monocytes over 50% was observed in all the three groups of mice. There were no significant differences among the three groups of mice.

We further examined the frequencies of CD4$^+$ T cell subsets by the intracellular cytokine staining of *in vitro* PMA/ionomycin-stimulated spleen cells. As shown in Table 2, *in vitro* stimulated CD4$^+$ T cells mainly produced TNFα and IFNγ while both IL-4 and IL-17 were produced by a limited population. When the frequencies of these cytokine-producing CD4$^+$ T cells were compared between untreated and MR16-1-treated groups of mice, the frequency of TNFα$^+$ T cells was significantly decreased in MR16-1-treated KO1 mice, while there was no difference in the frequencies of IFNγ$^+$ T cells, IL-4$^+$ T cells, and IL-17$^+$ T cells per CD4$^+$ T cells between the two groups of mice.

Table 1. Spleen weight, splenic lymphocyte subpopulations, and peripheral monocyte frequencies in untreated, normal rat IgG-treated, and MR16-1-treated KO1 mice.[a]

	None	Rat IgG	MR16.1
Spleen weight (gm)	0.18 ± 0.03	0.19 ± 0.04	0.18 ± 0.05
Spleen cell populations (%)			
B220$^+$B cells/total cells	60.0 ± 4.8	63.9 ± 0.8	66.1 ± 2.9
CD69$^+$B220$^+$ B cells/total B cells	5.6 ± 0.3	6.0 ± 1.2	2.2 ± 0.6[b]
PNA$^+$B220$^+$ B cells/total B cells	1.9 ± 0.8	2.3 ± 0.5	2.5 ± 0.2
CD138$^+$plasma cells/total cells	1.1 ± 0.6	0.7 ± 0.2	1.0 ± 0.2
CD3$^+$T cells/total cells	20.9 ± 6.0	20.0 ± 0.2	20.2 ± 3.7
CD69$^+$CD3$^+$ T cells/total T cells	29.3 ± 2.5	24.8 ± 2.2	24.6 ± 5.8
CD4$^+$ T cells/total cells	17.5 ± 0.4	16.2 ± 0.8	11.9 ± 0.7[b]
CD8$^+$ T cells/total cells	3.9 ± 0.4	5.2 ± 0.3	7.9 ± 2.9
CD4/CD8 ratio	4.6 ± 0.6	3.1 ± 0.0	1.9 ± 0.4[c]
CD25$^+$Foxp3$^+$ T cells/CD4$^+$ T cells	21.3 ± 1.4	23.2 ± 2.8	24.2 ± 3.5
Peripheral CD11b$^+$ monocytes (%)	54.3 ± 11.4	50.5 ± 11.9	56.9 ± 7.3

[a]Values are the mean ± SEM of at least six female mice aged 9–10 months.
[b]Differences were statistically significant versus KO1 ($P<0.01$) and versus normal rat IgG-treated KO1 ($P<0.05$).
[c]Differences were statistically significant versus KO1 ($P<0.05$).

qRT-PCR analysis of RANKL/OPG and cytokine/chemokine mRNA expression levels in ankle joints

To evaluate the transcription levels of RANKL, OPG, cytokines, and chemokines in ankle joint tissues, qRT-PCR analysis was performed using mRNA extracted from joint tissues of each of four 8~9-month-old mice from the three groups. Data of normal B6 mice were used as a relative control. The expression levels in the three groups of mice were evaluated as fold change compared with the level in B6 mice tentatively designated as 1. As shown in Figure 3a, the expression level of RANKL in MR16-1-treated KO1 mice was significantly lower than the levels in untreated and normal rat IgG-treated KO1 mice. As for the OPG expression levels, all the three groups showed the levels lower than the level in B6 mice. Nevertheless, when the levels were compared among the three groups, the level in MR16-1-treated KO1 mice was significantly higher than the levels in untreated and normal rat IgG-treated KO1 mice. Accordingly, when calculating the RANKL/OPG ratio (Figure 3b), the average ratio in MR16-1-treated KO1 mice was almost the same as that in normal B6 mice. This was in contrast to the findings in untreated and normal rat IgG-treated KO1 mice, in which these ratios were over 10 times higher than the ratio in normal B6 mice.

As MCP-1, RANTES, and CX3CL1 have been shown to be important chemokines involved in the pathogenesis of RA [29], we compared their expression levels in ankle joint tissues. As shown in Figure 3c, the MCP-1 expression levels were markedly up-regulated in untreated and normal rat IgG-treated KO1 mice with overt arthritis, while arthritis-free MR16-1-treated KO1 mice showed significantly lower levels. As for the RANTES expression levels, the three groups of mice showed low levels and there was no difference among them. It was noted that CX3CL1 expression levels in the three groups of mice were lower than the level in control B6 mice, and that the levels in untreated and normal rat IgG-treated KO1 mice with overt arthritis were significantly lower than that in arthritis-free MR16-1-treated KO1 mice. Thus, it appears

Table 2. Frequencies of CD4$^+$ T cell subsets in *in vitro* stimulated spleen cells in untreated and MR16-1-treated KO1 mice.[a]

	None	MR16.1
TNFα$^+$ T cells/total CD4$^+$ T cells	59.1 ± 2.0	50.3 ± 1.0[b]
IFNγ$^+$ T cells/total CD4$^+$ T cells	54.3 ± 4.4	55.1 ± 1.6
IL-4$^+$ T cells/total CD4$^+$ T cells	0.67 ± 0.2	0.38 ± 0.1
IL-17$^+$ T cells/total CD4$^+$ T cells	0.23 ± 0.05	0.23 ± 0.05

[a]Values are the mean ± SEM of at least four female mice aged 9 months.
[b]Differences were statistically significant versus KO1 ($P<0.05$).

For personal use only.

RIGHTSLINK

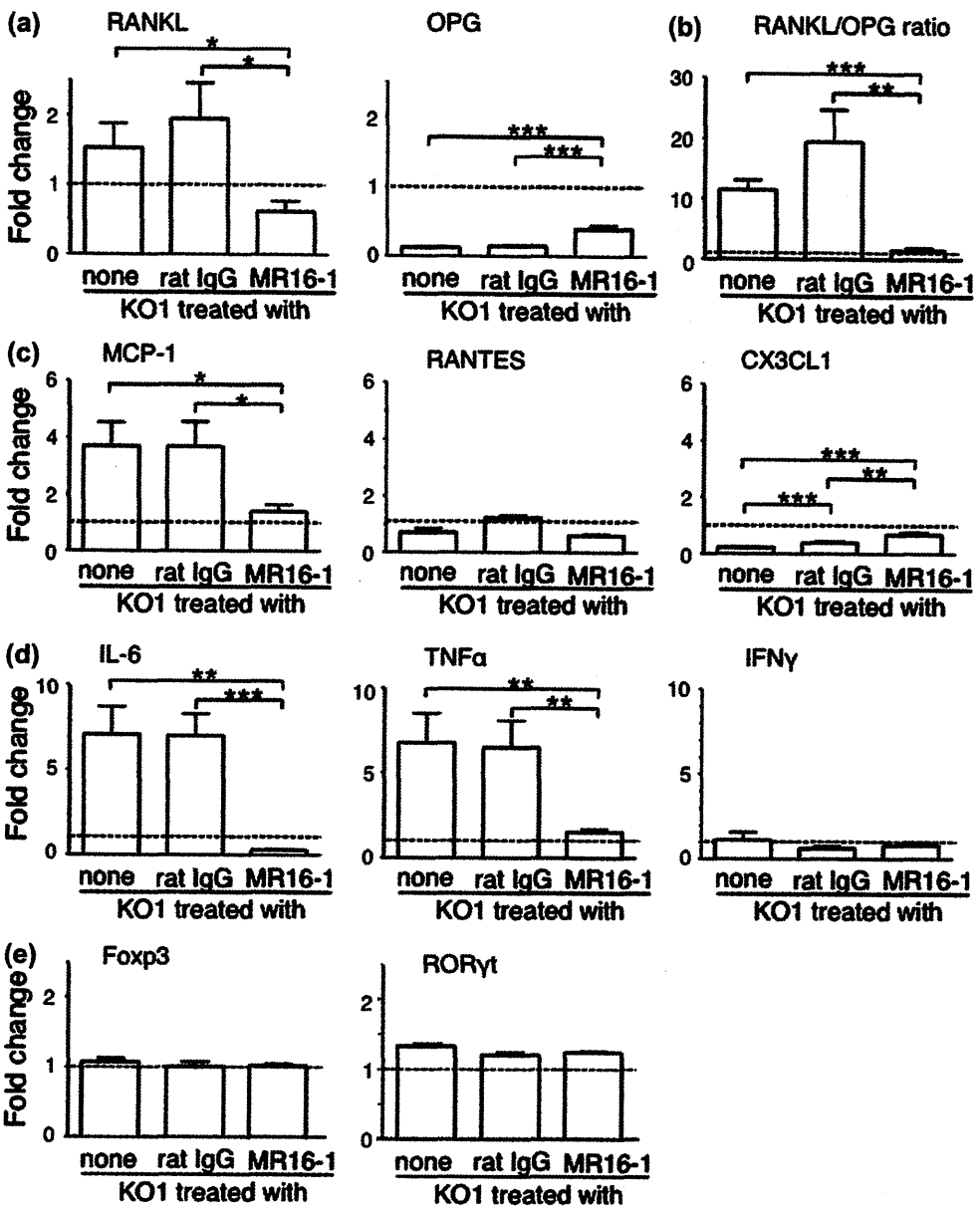

Figure 3. Comparisons of mRNA expression levels of (a) RANKL and OPG, (b) RANKL/OPG ratio, (c) MCP-1, RANTES, and CX3CL1, (d) IL-6, TNα and IFNγ, and (e) Foxp3 and RORγt in ankle joints by quantitative real-time PCR analysis among untreated, normal rat IgG-treated, and MR16-1-treated KO1 mice at 8–9 months of age. The value of normal B6 mice was designated as 1, and values of each of the three groups of mice were evaluated as fold change compared with the value in B6 mice. Data are shown as mean + SEM of four mice from each group. Statistical significance is shown (* $P<0.05$, ** $P<0.01$, *** $P<0.001$).

that MCP-1 plays a pivotal role in the process of inflammation in arthritic joints of KO1 mice.

Figure 3d compares the expression levels of IL-6, TNFα and IFNγ among the three groups of mice. The levels of IL-6 were markedly up-regulated in untreated and normal rat IgG-treated KO1 mice compared with the level in MR16-1-treated KO1 mice. Intriguingly, the IL-6 expression level in MR16-1-treated KO1 mice was to a great degree suppressed, even to below the level in normal B6 mice, suggesting that IL-6 secreting cells in ankle joints is under the control of autocrine mechanism [30]. The levels of TNFα were also markedly up-regulated in the former two arthritis-prone groups of mice, but the level in MR16-1-treated KO1 mice was the same as the level in normal B6 mice. IFNγ expression levels in the three groups were comparable to the level in B6 mice, and there was no difference in expression levels among the three groups. IL-17 expression was undetectable in ankle joint tissues from B6 and the three groups of mice in our experiment, as previously described [23].

Since IL-6 was shown to play an important role in the regulation of Th17/Treg cell balance [31], we examined the effect of IL-6 signal blockade on the expression levels of Foxp3 and RORγt, the transcription factors specific for the development of Treg cells and Th17 cells, respectively. The results showed that there was no *in vivo* effect of MR16-1 treatment on their expression levels in ankle joint tissues in our arthritis model (Figure 3e).

Therapeutic effect of MR16-1 treatment

To further examine the therapeutic effect of MR16-1 treatment, 7-month-old KO1 mice with arthritis of the score 1 or 2 were selected and divided into two groups. One group was treated with MR16-1 for 2 months and the other group was left untreated. The arthritis score in mice left untreated was increased with age; however, there was no such increase in the score in MR16-1-treated group of mice (Figure 4a).

We also evaluated the transcription levels of RANKL, OPG, MCP-1, IL-6, and TNFα in ankle joint tissues using qRT-PCR analysis. As in the case of preventive treatment, RANKL expression level was decreased and OPG expression level was increased in therapeutic MR16-1 treatment (Figure 4b), resulting in the significant decrease in RANKL/OPG ratio (Figure 4c), compared with the findings in untreated mice. In contrast, the therapeutic MR16-1 treatment showed no effect on the expression levels of MCP-1 (Figure 4d) and TNFα (Figure 4e) in ankle joint tissues, indicating that IL-6 signal blockade may be ineffective to suppress the ongoing inflammatory cytokine/chemokine production.

RIGHTSLINK

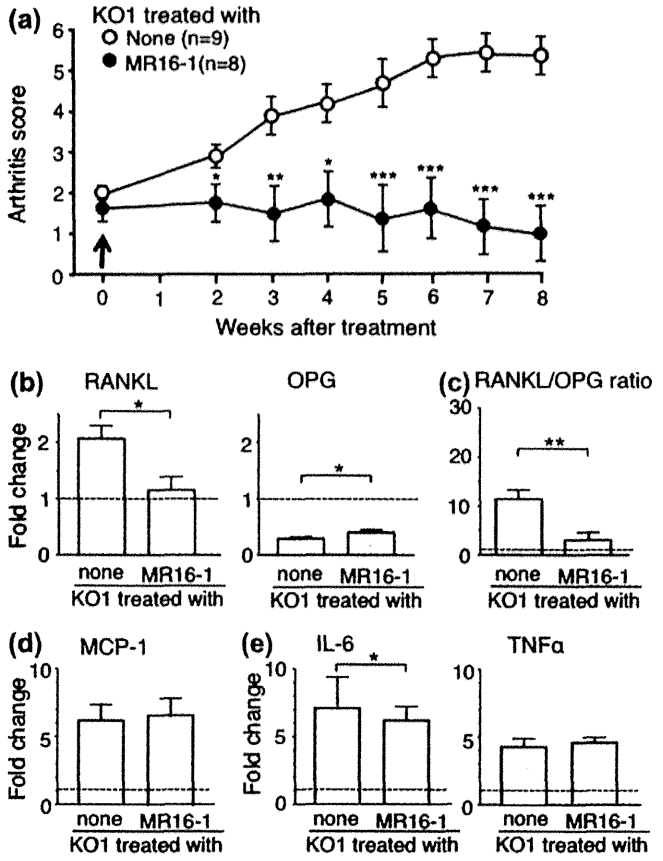

Figure 4. Therapeutic effect of MR16-1 treatment. (a) Seven-month-old KO1 mice with arthritis score 1 or 2 were treated or untreated with MR16-1 during 8 weeks. The sequential changes of arthritis score are shown. (b)–(e) Comparisons of mRNA expression levels of (b) RANKL and OPG, (c) RANKL/OPG ratio, (d) MCP-1, and (e) IL-6 and TNFα in ankle joints by quantitative real-time PCR analysis between untreated and MR16-1-treated KO1 mice at 9 months of age. The values were evaluated as fold change compared with the value in B6 mice, as shown in Figure 3. Data are shown as mean + SEM of four mice from each group. Statistical significance is shown (* $P<0.05$, ** $P<0.01$, *** $P<0.001$).

The IL-6 expression level was lower in MR16-1-treated mice than found in untreated mice; however, the level was much higher when compared with that in normal B6 mice (Figure 4e), the finding quite different from that in the case of preventive treatment (Figure 3d).

Discussion

The severity of arthritis spontaneously occurring in KO1 mice was markedly suppressed with the treatment of an inhibitory mAb against IL-6R, MR16-1. The marked synovitis with inflammatory cell infiltration, pannus formation, TRAP-positive osteoclast generation, and the destruction of cartilages and bones observed in untreated and normal rat IgG-treated KO1 mice were seldom observed in MR16-1-treated KO1 mice. This suppression was associated with the decrease in production of autoantibodies RF and anti-CCP. These findings clearly demonstrate that, in addition to the role in enhancing the autoantibody production, IL-6 plays a pivotal role in the inflammatory response and osteoclastogenesis in arthritic tissues in KO1 mice. It was notable that, when the average ratio of RANKL to OPG expression levels in joint tissues was examined, while the ratios in arthritis-prone untreated and normal rat IgG-treated KO1 mice were both over 10 times higher than the ratio in normal B6 mice, such aberrant ratios were ameliorated in KO1 mice with both preventive and therapeutic treatments of MR16-1. As OPG is a decoy receptor for RANKL and suppresses RANKL-mediated osteoclastogenesis [3], normalization of the aberrantly high RANKL/OPG ratio appears to be responsible for the protective effect of MR16-1 on the joint destruction.

RA is an autoantibody-mediated autoimmune disease, in which IgG immune complexes (ICs) may trigger the joint inflammation and induce a marked cellular infiltrate including macrophages, mast cells, $CT4^+$ T cells, $CD8^+$ T cells, and B cells. The exact mechanisms for the inflammatory cell infiltration are unidentified; however, it appears that inflammatory cytokines/chemokines play a pivotal role for the disease progression [4]. Our arthritis-prone KO1 mice lack the expression of inhibitory FcγRIIB, which is usually expressed on B cells and most cells of myeloid lineage including macrophages. The lack of FcγRIIB expression on B cells induces the breakdown of self-tolerance and the production of IgG autoantibodies [32]. The resultant IgG ICs formed in the joint tissues stimulate macrophages via activated IgG Fc receptors to produce several kinds of inflammatory cytokines, such as TNFα and IL-6 [4]. This step may be augmented in KO1 mice, since KO1 macrophages lack inhibitory FcγRIIB. Thus, it is feasible to speculate that activated macrophages play a pivotal role in the pathogenesis of arthritis in KO1 mice. This is consistent with the present study as well as our previous study [23], showing that both IL-6 and TNFα are indispensable in arthritis of KO1 mice.

IL-6 is a multifunctional cytokine. It was originally identified as a B-cell differentiation factor that induces the terminal maturation of B cells into antibody-producing plasma cells. However, later studies have shown that IL-6 acts to activate and differentiate not only B cells but also T cells, hepatocytes, and hematopoietic progenitor cells [33]. In the present study, the MR16-1 treatment resulted in down-regulation of autoantibody production associated with the decrease in the frequency of $CD69^+$ activated B cells as well as in the frequency of $CD4^+$ T cells in the spleen. Intracellular cytokine staining analysis revealed that the frequency of TNFα-producing $CD4^+$ T cells was decreased in MR16-1-treated mice. Although IL-6 was shown to regulate Th17/Treg cell balance [31], our qRT-PCR and intracellular cytokine staining analysis in our model revealed that there was no detectable *in vivo* effect of IL-6 signal blockade on this balance. It has been reported that osteoclast precursors arise from the monocyte/macrophage lineage of cells derived from hematopoietic progenitor cells [27] and that IL-6 increases osteoclast precursor recruitment through activating hematopoietic progenitor cells [33]. In the present study, however, the MR16-1 treatment did not affect the frequencies of peripheral monocytes in the blood, suggesting that the mechanisms of growth and differentiation of osteoclast progenitors are more complex.

IL-6 signal is mediated through a protein complex including the membrane-bound, non-signaling α-receptor subunit (IL-6R) and two signal-transducing gp130 subunits [33]. IL-6R is predominantly expressed on hepatocytes, myeloid derived cells, and some lymphocytes, while gp130 is expressed ubiquitously [34]. IL-6 transduces signals via membrane-bound IL-6R and signal-transducing gp130 subunits; however, IL-6 signals can also be transduced via soluble IL-6R (sIL-6R) by the association with ubiquitously expressed gp130 [34,35]. Mice with a gain-of-function mutation of gp130 were shown to develop arthritis due to the excess IL-6 signal [36], supporting the important role of IL-6 in the pathogenesis of RA. It was reported that, while neither IL-6 nor sIL-6R alone stimulates bone resorption, a combined effect of IL-6 and sIL-6R enhanced bone resorption in association with the up-regulated expression of RANKL in mouse calvaria bone explants [37]. Because this effect was blocked by neutralizing antibody against gp130, RANKL-producing cells are suggested to express gp130.

In the previous study, we found that the arthritis-free TNFα-deficient KO1 mice showed the same level of RANKL expression in joint tissues as that found in KO1 mice with overt arthritis [23]. This is in contrast to the present findings, in which the RANKL

For personal use only.

RIGHTSLINK

expression level in arthritis-free MR16-1-treated KO1 mice was significantly lower than the levels in arthritis-prone untreated and rat IgG-treated KO1 mice. Thus, it appears that IL-6, but not TNFα, may transduce signals to enhance the expression level of RANKL. This is consistent with the report showing that IL-6/sIL-6R but not TNFα directly induces RANKL expression in fibroblast-like synoviocytes from RA patients [38]. On the other hand, the current as well as our earlier studies [23] showed that the expression levels of OPG were markedly down-regulated in arthritis-prone untreated and normal rat IgG-treated KO1 mice. OPG is produced by a variety of cells including osteoblasts, B cells, dendritic cells, and vascular endothelial cells [39,40]. Marked decrease in OPG expression in arthritic joints is suggested to be due to the exhaustion of OPG production over extended periods of chronic stimulation by TNFα [40]. Consistently, synovial OPG expression levels were increased in anti-TNFα-treated RA patients [41] as well as in TNFα-deficient KO1 mice [23]. In the present study, MR16-1 treatment restored the OPG expression in joint tissues. This restoration in mice with the preventive treatment of MR16-1 may be due to the down-regulated expression of TNFα. Alternatively, IL-6 may contribute to the suppression of OPG expression independent of the effect of TNFα, since Liu et al. [42] reported that IL-6 mediates the inhibitory effects on OPG production via the increased secretion of prostaglandin E2. In our therapeutic model, the TNFα expression levels were comparable between the MR16-1-treated and untreated KO1 mice; nonetheless, the treated mice showed lower IL-6 and higher OPG expressions in ankle joint tissues than the findings in untreated mice, suggesting that the change in OPG expression in joint tissues may be independent of the effect of TNFα.

In hierarchical relationships within cytokine networks involved in the pathogenesis of RA, a linear model has been proposed, in which TNFα would drive downstream cytokine generation, such as IL-1 and IL-6, sequentially [43]. The present study showed that, while the IL-6 signal blockade was ineffective to suppress the ongoing TNFα production, this blockade in the preclinical stages reduced the TNFα expression in joint tissues, suggesting the presence of another pathway of cytokine network. Intriguingly, it has been shown that the serum IL-6 level is increased in tocilizumab-treated RA patients [44]. This increase was suggested to be mainly due to the decreased IL-6R-mediated degradation of IL-6, since IL-6 mRNA expression in synovial biopsy samples was rather decreased after administration of tocilizumab [45]. This is consistent with the finding in the current study that IL-6 mRNA expression level in ankle joint tissues was decreased in MR16-1-treated mice, as compared with that in untreated mice. However, because the IL-6 mRNA level in mice with the preventive MR16-1 treatment was much lower than that found in mice with the therapeutic treatment, it is likely that the blockade of IL-6 signals in earlier stages of arthritis is more effective to suppress inflammatory cytokines, such as TNFα and IL-6.

Since RA is a chronic autoimmune disease developing under the regulation of multiple susceptibility factors, it is plausible that different sets of proinflammatory cytokines/chemokines may be involved in the pathogenesis of RA particularly in different clinical and pathological stages. As the same RA phenotype may develop under different mechanisms, it is also plausible that different sets of proinflammatory cytokines/chemokines may cause phenotypically similar clinical subsets of RA. Our arthritis-prone KO1 mouse model, as well as others, is one of the most useful mouse models for clarifying the mechanisms of ongoing crosstalk of causative cytokines/chemokines in the pathogenesis of various subsets of RA, in order to search for a tailor-made therapy against this complex chronic autoimmune disease.

Acknowledgments

This work was supported in part by a Grant-in-Aid (24590491) from the Ministry of Education, Science, Technology, Sports and Culture of Japan and a grant for Research on Intractable Diseases from the Ministry of Health, Labour and Welfare of Japan.

Conflict of interest

N. Nishimoto has received research grants, consultant fees, and/or speakers' bureau honoraria from Chugai Pharmaceutical Co. Ltd., Bristol-Myers Squibb, Eisai Co. Ltd., Janssen Pharmaceutical KK, and F. Hoffmann-La Roche.

References

1. Walsh MC, Kim N, Kadono Y, Rho J, Lee SY, Lorenzo J, Choi Y. Osteoimmunology: interplay between the immune system and bone metabolism. Annu Rev Immunol. 2006;24:33–63.
2. Takayanagi H. Osteoimmunology and the effect of the immune system on bone. Nat Rev Rheumatol. 2009;5(12):667–76.
3. Simonet WS, Lacey DL, Dunstan CR, Kelley M, Chang MS, Luthy R, et al. Osteoprotegerin: a novel secreted protein involved in the regulation of bone density. Cell. 1997;89(2):309–19.
4. McInnes JB, Schett G. Cytokines in the pathogeneses of rheumatoid arthritis. Nat Rev Immunol. 2007;7(6):429–42.
5. Breedveld FC, Emery P, Keystone E, Patel K, Furst DE, Kalden JR, et al. Infliximab in active early rheumatoid arthritis. Ann Rheum Dis. 2004;63(2):149–55.
6. Fleischmann RM, Schechtman J, Bennett R, Handel ML, Burmester GR, Tesser J, et al. Anakinra, a recombinant human interleukin-1 receptor antagonist (r-metHuIL-1ra), in patients with rheumatoid arthritis: A large, international, multicenter, placebo-controlled trial. Arthr Rheum. 2003;48(4):927–34.
7. Voll RE, Kalden JR. Do we need new treatment that goes beyond tumor necrosis factor blockers for rheumatoid arthritis? Ann N Y Acad Sci. 2005;1051:799–810.
8. van den Berg WB, McInnes IB. Th17 cells and IL-17 A-Focus on immunopathology and immunotherapeutics. Semin Arthritis Rheum. 2013;43(2):158–70.
9. Thorbecke GJ, Shah R, Leu CH, Kuruvilla AP, Hardison AM, Palladino MA. Involvement of endogenous tumor necrosis factor α and transforming growth factor β during induction of collagen type II arthritis in mice. Proc Natl Acad Sci USA. 1992;89(16):7375–9.
10. Piguet PF, Grau GE, Vesin C, Loetscher H, Gentz R, Lesslauer W. Evolution of collagen arthritis in mice is arrested by treatment with antitumour necrosis factor (TNF) antibody or a recombinant soluble TNF receptor. Immunology. 1992;77(4):510–4.
11. Campbell IK, O'Donnell K, Lawlor KE, Wicks IP. Severe inflammatory arthritis and lymphadenopathy in the absence of TNF. J Clin Invest. 2001;107(12):1519–27.
12. Ji H, Pettit A, Ohmura K, Oriz-Lopez A, Duchatelle V, Degott C, et al. Critical roles for interleukin 1 and tumor necrosis factor α in antibody-induced arthritis. J Exp Med. 2002;196(1):77–85.
13. Hirota K, Hashimoto M, Yoshitomi H, Tanaka S, Nomura T, Yamaguchi T, et al. T cell self-reactivity forms a cytokine milieu for spontaneous development of IL-17$^+$ Th cells that cause autoimmune arthritis. J Exp Med. 2007;204(1):41–7.
14. Nakae S, Saijo S, Horai R, Sudo K, Mori S, Iwakura Y. IL-17 production from activated T cells is required for the spontaneous development of arthritis in mice deficient in IL-1 receptor antagonist. Proc Natl Acad Sci USA. 2003;100(10):5986–90.
15. Nakae S, Nambu A, Sodo K, Iwakura Y. Suppression of immune induction of collagen-induced arthritis in IL-17-deficient mice. J Immunol. 2003;171(11):6173–7.
16. Doodes PD, Cao Y, Hamel KM, Wang Y, Farkas B, Iwakura Y, et al. Development of proteoglycan-induced arthritis is independent of IL-17. J Immunol. 2008;181(1):329–37.
17. Mima T, Nishimoto N. Clinical value of blocking IL-6 receptor. Curr Opin Rheumatol. 2009;21(3):224–30.
18. Smolen JS, Beaulieu A, Rubbert-Roth A, Ramos-Remus C, Rovensky J, Alecock E, et al. Effect of interleukin-6 receptor inhibition with tocilizumab in patients with rheumatoid arthritis (OPTION study): a double-blind, placebo-controlled, randomised trial. Lancet. 2008;371(9617):987–97.
19. Dougados M, Kissel K, Sheeran T, Tak PP, Conaghan PG, Mola EM, et al. Adding tocilizumab or switching to tocilizumab monotherapy

RIGHTSLINK

in methotrexate inadequate responders: 24-week symptomatic and structural results of a 2-year randomised controlled strategy trial in rheumatoid arthritis (ACT-RAY). Ann Rheum Dis. 2013;72(1):43–50.
20. Takagi N, Mihara M, Moriya Y, Nishimoto N, Yoshizaki K, Kishimoto T, et al. Blockage of interleukin-6 receptor ameliorates joint disease in murine collagen-induced arthritis. Arthr Rheum. 1998;41(12):2117–21.
21. Kagari T, Doi H, Shimozato T. The importance of IL-1β and TNF-α, and the non-involvement of IL-6, in the development of monoclonal antibody-induced arthritis. J Immunol. 2002;169(9):1459–66.
22. Sato-Hayashizaki A, Ohtsuji M, Lin Q, Hou R, Ohtsuji N, Nishikawa K, et al. Presumptive role of 129 strain-derived *Sle16* locus in rheumatoid arthritis in a new mouse model with Fcγ receptor Type IIb-deficient C57BL/6 genetic background. Arthr Rheum.2011;63(10):2930–8.
23. Okazaki H, Lin Q, Nishikawa K, Ohtsuji N, Tsurui H, Ohtsuji M, et al. TNFα but not IL-17 is critical in the pathogenesis of rheumatoid arthritis spontaneously occurring in a unique FcγRIIB-deficient mouse model. Modern Rheum. DOI: 10.3109/14397595.2014.886351
24. Takai T, Ono M, Hikida M, Ohmori H, Ravetch JV. Augmented humoral and anaphylactic responses in FcγRII-deficient mice. Nature. 1996;379(6563):346–9.
25. Tamura T, Udagawa N, Takahashi N, Miyaura C, Tanaka S, Yamada Y, et al. Soluble interleukin-6 receptor triggers osteoclast formation by interleukin-6. Proc Natl Acad. Sci USA. 1993;90(24):11924–8.
26. Abe Y, Ohtsuji M, Ohtsuji N, Lin Q, Tsurui H, Nakae S, et al. Ankylosing enthesitis associated with up-regulated IFN-γ and IL-17 production in (BXSB × NZB) F1 male mice: a new mouse model. Mod Rheumatol. 2009;19(3):316–22.
27. Gordon S, Taylor PR. Monocyte and macrophage heterogeneity. Nat Rev Immunol. 2005;5(12):953–64.
28. Kikuchi S, Santiago-Raber M-L, Amano H, Amano E, Fossati-Jimack L, Moll T, et al. Contribution of NZB autoimmunity 2 to Y-linked autoimmune acceleration-induced monocytosis in association with murine systemic lupus. J Immunol. 2006;176(5):3240–7.
29. Iwamoto T, Okamoto H, Toyama Y, Momohara S. Molecular aspects of rheumatoid arthritis: chemokines in the joints of patients. FEBS J. 2008;275(18):4448–55.
30. Yu RY-L, Wang X, Pixley FJ, Yu J, Dent AL, Broxmeyer DH, et al. BCL-6 negatively regulated macrophage proliferation by suppressing autocrine IL-6 production. Blood. 2005;105(4):1777–84.
31. Steinman L. A brief history of T_H17, the first major revision in the T_H1/T_H2 hypothesis of T cell-mediated tissue damage. Nat Med. 2007:13(2);139–45.
32. Bolland S, Ravetch JV. Spontaneous autoimmune disease in FcγRIIB-deficient mice results from strain-specific epistasis. Immunity. 2000;13(2):277–85.
33. Kishimoto T, Akira S, Narazaki M, Taga T. Interleukin-6 family of cytokines and gp130. Blood. 1995;86(4):1243–54.
34. Rose-John S, Scheller J, Elson G, Jones SA. Interleukin-6 biology is coordinated by membrane-bound and soluble receptors: role in inflammation and cancer. J Leukoc Biol. 2006;80(2):227–36.
35. Dayer J-M, Choy E. Therapeutic targests in rheumatoid arthritis: the interleukn-6 receptor. Rheumatology. 2010;49(1):15–24.
36. Atsumi T, Ishihara K, Kamimura D, Ikushima H, Ohtani T, Hirota S, et al. A point mutation of Tyr-759 in interleukin 6 family cytokine receptor subunit gp130 causes autoimmune arthritis. J Exp Med. 2002;196(7):979–90.
37. Palmqvist P, Persson E, Conaway HH, U.H. Lerner UH. IL-6, leukemia inhibitory factor, and oncostatin M stimulate bone resorption and regulate the expression of receptor activator of NF-κB in mouse calvariare. J Immunol. 2002;169(6):3353–62.
38. Hashizume M, Hayakawa N. Mihara M. IL-6 trans-signalling directly induces RANKL on fobroblast-like synovial cells and is involved in RANKL induction by TNF-α and IL-17. Rheumatology. 2008;47(11):1635–40.
39. Yun TJ, Chaudhary PM, Shu GL, Frazer JK, Ewing MK, Schwartz SM, et al. OPG/FDCR-1, a TNF receptor family member, is expressed in lymphoid cells and is up-regulated by ligating CD40. J Immunol. 1998;161(11):6113–21.
40. Zannettio ACW, Holding CA, Diamond P, Atkins GJ, Kostakis P, Farrugia A, et al. Osteoprotegerin (0PG) is localized to the Weibel-Palade bodies of human vascular endothelial cells and is physically associated with von Willebrand factor. J Cell Physiol. 2005;204(2):714–23.
41. Catrina AI, af Klint E, Ernestam S, Catrina S-B, Makrygiannakis D, Botusan IR, et al. Anti-tumor necrosis factor therapy increases synovial osteoprotegerin expression in rheumatoid arthritis. Arthr Rheum. 2006;54(1):76–81.
42. Liu XH, Kirschenbaum A, Yao S, Levine AC. Interactive effect of interleukin-6 and prostaglandin E2 on osteoclastogenesis via the OPG/RANKL/RANK system. Annn N Y Acad Sci. 2006;1068:225–33.
43. Feldmann M, Brennan FM, Maini RN. Rheumatoid Arthritis. Cell. 1996;85(3):307–10.
44. Nishimoto N, Terao K, Mima T, Nakahara H, Takagi N, Kakehi T. Mechanisms and pathologic significances in increase in serum interleukin-6 (IL-6) and soluble receptor after administration of an anti-IL-6 receptor antibody, tocilizumab, in patients with rheumatoid arthritis and Castleman disease. Blood. 2008;112(10):3959–64.
45. Ducreux J, Durez P, Galant C, Toukap AN, Van de Eynde B, Houssiau FA, et al. Global molecular effects of tocilizumab therapy in rheumatoid arthritis synovium. Arthr Rheum. 2014; 66(1):15–23.

For personal use only.

RIGHTSLINK

Kanari et al. BMC Immunology 2014, 15:47
http://www.biomedcentral.com/1471-2172/15/47

BMC Immunology

RESEARCH ARTICLE Open Access

Dichotomy in FcγRIIB deficiency and autoimmune-prone SLAM haplotype clarifies the roles of the Fc receptor in development of autoantibodies and glomerulonephritis

Yasuyoshi Kanari[1], Akiko Sugahara-Tobinai[1], Haruka Takahashi[1], Masanori Inui[1], Akira Nakamura[1,2], Sachiko Hirose[3] and Toshiyuki Takai[1*]

Abstract

Background: The significance of a unique inhibitory Fc receptor for IgG, FcγRIIB (RIIB), in the prevention of spontaneous production of autoantibodies remains controversial, due mainly to the fact that the *RIIB* locus is adjacent to the autoimmune-related *SLAM* locus harboring the genes coding for signaling lymphocyte activation molecules, making it difficult to isolate the effect of RIIB deletion from that of *SLAM* in gene-targeted mice. Our objective was to determine the influence of *RIIB* deletion on the spontaneous development of autoimmune diseases and to compare it with that of potentially pathogenic *SLAM*.

Results: We established two congenic C57BL/6 (B6) strains, one with the *RIIB* deletion and the other with *SLAM*, by backcrossing 129/SvJ-based *RIIB*-deficient mice into the B6 genetic background extensively. The RIIB deficiency indeed led to the production and/or accumulation of a small amount of anti-nuclear autoantibodies (ANAs) and to weak IgG immune-complex deposition in glomeruli without any obvious manifestation of lupus nephritis. In contrast, pathogenic *SLAM* in the B6 genetic background induced ANAs but no IgG immune-complex deposition in the kidneys. Naïve *SLAM* mice but not RIIB-deficient mice exhibited hyperplasia of splenic germinal centers.

Conclusion: The present results clarify the roles of RIIB in preventing production and/or accumulation of a small amount of ANAs, and development of glomerulonephritis. The combined effects of RIIB deletion and pathogenic SLAM can lead to severe lupus nephritis in the B6 genetic background.

Keywords: Autoimmune disease, Systemic lupus erythematosus, Autoantibody production, B cells, Myeloid cells, Inhibitory receptor

Background

Systemic lupus erythematosus (SLE) is characterized by spontaneous production of autoantibodies including anti-nuclear autoantibodies (ANAs), and by development of vasculitis and autoimmune glomerulonephritis (so-called lupus nephritis) preferentially in females. The genetic susceptibility loci have been mapped throughout the chromosomes, the major locus having been mapped to the chromosome 1 telomeric region, in which many immunoregulatory genes are concentrated in humans as well as in mice [1-3]. One of the major susceptible haplotypes in this region has been identified in murine SLE models as the group of seven genes for the signal lymphocyte activation molecule (SLAM or CD2) family members, which regulate cognate interactions between T and B cells, and signaling [4]. Interestingly, while both SLAM haplotypes 1 and 2 in non-autoimmune strains of mice, such as C57BL/6 (B6) and 129/SvJ, respectively, are not harmful when expressed in the original genetic backgrounds of the host strains, SLAM haplotype 2 in 129 mice ($SLAM^{129}$) renders the hosts susceptible to autoimmunity, ANAs being produced when expressed in the B6 genetic background

* Correspondence: tostakai@idac.tohoku.ac.jp
[1]Department of Experimental Immunology and CREST Program of JST, Institute of Development, Aging and Cancer, Tohoku University, 4-1 Seiryo, Sendai 980-8575, Japan
Full list of author information is available at the end of the article

BioMed Central

© 2014 Kanari et al.; licensee BioMed Central Ltd. This is an Open Access article distributed under the terms of the Creative Commons Attribution License (http://creativecommons.org/licenses/by/4.0), which permits unrestricted use, distribution, and reproduction in any medium, provided the original work is properly credited. The Creative Commons Public Domain Dedication waiver (http://creativecommons.org/publicdomain/zero/1.0/) applies to the data made available in this article, unless otherwise stated.

[4,5]. Interestingly, four members of the SLAM family cluster, *Cd48*, *Ly108*, *Cd84*, and *Cs1*, vary in their expression in splenic B and/or T cells between B6 mice harboring haplotypes 1 and 2 [4]. In particular, Ly108 was suggested to be one of the determinants of the autoimmunity susceptibility [4,6].

Another important susceptible gene for autoimmunity in this 1q telomeric region has been suggested to be the gene coding for a unique inhibitory Fc receptor for IgG (FcγR), FcγRIIB (RIIB) [7-11]. Generally, it is well established that the FcγR family molecules expressed on myeloid-lineage cells and B cells play crucial roles in adaptive immune responses and inflammation, in which activating-type FcγRs such as FcγRIII initiate and accelerate the responses, while inhibitory RIIB decreases them upon co-engagement with other activating-type FcγRs or B cell antigen receptors via IgG immune complexes (IgG-ICs) [7,9-12]. Thus, RIIB executes important IgG-mediated feedback regulation of cell activation, proliferation and antibody/cytokine production, as demonstrated in different experimental settings using RIIB-deficient ($RIIB^{-/-}$) mice [13-15]. In contrast to this well-established feedback regulation, the roles of RIIB in maintaining tolerance and in preventing spontaneous development of autoimmunity, however, remain uncertain due to the inconsistent phenotypes observed in $RIIB^{-/-}$ mice by different research groups, particularly in terms of the level of ANAs and the severity of lupus nephritis [8,16-18]. In addition, a recent report [19] pointed out the role of RIIB expressed in liver sinusoidal endothelial cells in the clearance of small size IgG-ICs, so the additional RIIB function of minimizing the level of pathologic IgG-ICs in the blood should also be taken into account.

Importantly, the *FcR* locus is adjacent to the *SLAM* locus in the 1q telomere of the mouse genome [1,4]. It has been pointed out that special care should be taken when examining the precise influence of any targeted gene, such as that of RIIB, located in this region on the occurrence of spontaneous autoantibody production and of lupus nephritis, by eliminating any influence of SLAM members in gene-targeted mice generated with 129-derived ES cells and backcrossed into the genetic background of B6 [1,4,5]. Therefore, the differences in the observed phenotypes in $RIIB^{-/-}$ mice could be due, at least in part, to the heterogeneity of the genomic interval around the $RIIB^{-/-}$ locus in the B6 background, which might be co-segregated with the autoimmune-prone $SLAM^{129}$ haplotype discussed above [4,6]. In addition to the genetic heterogeneity of $RIIB^{-/-}$ mice, unidentified differences in environmental conditions such as those in nutrition and the gut microbial flora should also be considered.

To clarify the role of RIIB in peripheral tolerance in the absence of any effect of the pathogenic $SLAM^{129}$ haplotype, we separated the $RIIB^{-/-}$ locus and the $SLAM^{129}$ locus by extensively backcrossing our $RIIB^{-/-}$ mice into the B6 background, followed by analysis of microsatellite markers in this genetic interval in the offspring. Each of the two congenic B6 strains obtained, one harboring $RIIB^{-/-}$ and the other pathogenic $SLAM^{129}$, exhibited unique phenotypes as to germinal center formation in the spleen, ANAs in serum, IgG-IC deposition in the kidneys, and development of lupus nephritis, which revealed the exact roles of RIIB and $SLAM^{129}$-derived set of molecules in maintaining tolerance, which were examined in detail in this study.

Methods

Mice

The original FcγRIIB (RIIB)-deficient mice constructed with a 129 and B6 hybrid background [13] were backcrossed into the B6 background for 12 generations as described previously [16] using C57BL/6NCrj mice (Charles River Inc. Japan, Kanagawa, Japan), and then, in this study, they were further backcrossed up to the 28th generation (Additional file 1: Figure S1A). The offspring were genotyped by analysis of simple sequence length polymorphisms (SSLP) using the seventeen SSLP markers on chromosome 1, which allow discrimination of the polymorphisms in B6 and 129 mice, particularly around the *Fcgr2b* gene and for the *SLAM* haplotype (Additional file 1: Figure S1). SSLP analysis was conducted by the Central Institute of Experimental Animals (Kawasaki, Japan). We established two substrains, N22 and N28 B6.$RIIB^{-/-}SLAM^{B6}$ ($RIIB^{-/-}$) and B6.$RIIB^{+/+}SLAM^{129}$ ($SLAM^{129}$) mice as well as N28 B6.$RIIB^{-/-}SLAM^{129}$ ($RIIB^{-/-}SLAM^{129}$) mice as controls (Additional file 1: Figure S1). RIIB-deficient mice were also provided by S. Hirose of Juntendo Univ. (Tokyo), or purchased from TACONIC® Farms (Germantown, NY, USA). When pertinent, we refer to our N28 $RIIB^{-/-}$ mice used in the present study as $RIIB^{-/-}$SENDAI and those obtained or purchased from others as $RIIB^{-/-}$TOKYO or $RIIB^{-/-}$TACONIC, respectively, in order to distinguish the data in figures. In several experiments, we also employed B6 mice obtained from CLEA Japan, Inc. (Tokyo, Japan) as aged controls or a 12-month-old NZB/W F_1 female mouse from Japan SLC, Inc. (Shizuoka, Japan) as an autoimmune control. For adaptation, the B6 mice of non-littermate controls and NZB/W F_1, $RIIB^{-/-}$TOKYO, and $RIIB^{-/-}$TACONIC mice were housed in our facility for at least 6 months before use. All mice were housed in the Experimental Animal Facility of The Institute of Development, Aging and Cancer (Tohoku University, Sendai, Japan), an environmentally controlled and specific pathogen-free facility. All animal protocols were reviewed and approved by the Animal Studies Committee of the Tohoku University, and we followed the guidelines defined by the committee.

Genotyping of SNPs

For isolation of genomic DNA samples, tail tips from mice were lysed by incubation in 100 μl of tail lysis buffer [50 mM Tris-HCl (pH8.0), 20 mM NaCl, 1 mM EDTA, 0.063% SDS and 1 mg/ml proteinase K] for at least 4 hours at 55°C. Tail lysates were diluted with 10 volumes of water, and then subjected to PCR amplification using gene-specific PCR primer pairs (Additional file 1: Table S1) and KOD FX polymerase (TOYOBO Co. Ltd., Osaka, Japan) as follows: initial 2-min incubation at 94°C, 30 cycles consisting of 95°C for 30 s, 60°C for 30 s and 72°C for 90 s, and a final 10 min elongation step at 72°C. For determination of SNPs in the vicinity of the *Fcgr2b* locus, PCR products were directly sequenced using specific primers (Additional file 1: Table S1) with a 3130x1 Sequencer (Life Technologies, Waltham, MA, USA).

Antibodies

For FACS analysis, the following fluorochrome-labeled antibodies specific for mouse molecules were used: CD4-FITC, CD4-Alexa647, CD19-Pacific blue (BioLegend, Inc., San Diego, CA, USA), and GL7-FITC and FAS-PE (Becton Dickinson Ltd., Franklin Lakes, NJ, USA). For immunohistochemistry, anti-mouse-IgM-Alexa488, anti-rat-IgG-Alexa488, and anti-mouse-IgG-Alexa555 (Invitrogen Life Technologies, Carlsbad, CA, USA), anti-mouse-IgD-biotin (BioLegend), GL7-Alexa488 (eBiosciences Inc., San Diego, CA, USA), and anti-mouse IgM F(ab')$_2$ Alexa647 (Jackson ImmunoResearch laboratories Inc., West grove, PA, USA) were used.

Histological study and immunohistochemistry

Kidneys were fixed with 4% paraformaldehyde in phosphate buffer. Specimens were embedded in paraffin, sectioned at 2 μm, and then stained with hematoxylin and eosin (HE) or periodic acid-Schiff (PAS). To evaluate glomerular lesions, at least 25 glomeruli were examined per HE-stained section by light microscopy based on pathological manifestations of inflammation, and/or tissue damage in a blind manner [20]. The severity of glomerulonephritis was estimated as follows; grade 0, normal; grade 1, neutrophil infiltration and segmental mesangial proliferation; grade 2, limited lobulated glomeruli in grade 1; and grade 3, crescent formation and severe lobulated glomeruli with lymphocyte infiltration (Additional file 1: Figure S2). To assay IgG-ICs deposition, kidney samples were embedded in O.C.T. compound (Tissue-Tek, Miles, Inc., Elkhart, IN), snap-frozen in liquid nitrogen, and then sectioned at 5 μm. The sections were fixed with 4% paraformaldehyde for 20 min, washed again three times with PBS, and then preincubated for 1 hour at room temperature with PBS containing 20% BSA to block nonspecific antibody binding. They were then incubated overnight at room temperature with affinity-purified Alexa488-conjugated goat F(ab')$_2$ fragments (H + L chain) anti-mouse IgG (Invitrogen). After washing three times with PBS, slides were mounted and examined under an Olympus BX50 microscope equipped with an Olympus BH2-RFL-T3 mercury lamp and appropriate optics.

Spleens were embedded in O.C.T. compound, frozen in liquid nitrogen, and then sectioned at 8 μm. Sections were fixed with acetone for 20 min at −20°C and then air-dried for 1 hour. After washing with PBS six times, sections were pre-incubated for 1 hour at room temperature with PBS containing 2% BSA for blocking, and then incubated with Alexa488-labeled anti-mouse IgM (Invitrogen) or Alexa488-labeled GL7, and biotinylated anti-mouse IgD (eBiosciences) for staining of splenic B cells. After washing with PBS three times, sections were incubated with 1:2000 diluted Alexa546-conjugated streptavidin at 4°C for 30 min.

Determination of ANA levels in sera from indirect immunofluorescence and by HEp2 cell staining combined with ELISA

For determination of gross ANA levels, serum samples from 24–48-wk-old mice were serially diluted from 1:40 to 1:320 with PBS containing 1% BSA. HEp-2 cell-seeded slides (Fluoro HEPANA test; MBL, Nagoya, Japan) were incubated with diluted serum samples for 45 min at room temperature, followed by brief washing and incubation with PBS for 60 min. Anti-nuclear antibodies (ANA) were detected with Alexa488-labeled anti-mouse IgG F(ab')$_2$ (Invitrogen Life Technologies) and visualized under a fluorescence microscope (Olympus, Tokyo, Japan). To determine ANA levels and the IgG isotypes by ELISA, sera from mice were diluted 1:100 with PBS containing 1% BSA and then added to a HEp-2 coated 96-well plate (ANA HEp Screen ELISA kit; Abnova, Taipei, Taiwan). ANA and the IgG isotypes were detected with HRP-conjugated goat anti-mouse IgG Fc fragment and anti-mouse IgG itsotype-specific antibodies (Bethyl Laboratory Inc., TX, USA), respectively.

ELISA measurement of Igs and anti-DNA antibodies

The serum levels of total IgM, IgG, and autoantibodies were measured by ELISA. For anti-ssDNA and -dsDNA antibodies, high-bound flat-bottom 96-well plates were coated firstly with 0.001% protamine sulfate in water for 60 min, and then with 5 μg/ml of single-strand or double-strand calf thymus DNA (SIGMA) diluted in 0.015 M sodium citrate containing 0.15 M NaCl for 90 min, followed by blocking with 50% FCS in PBS for 60 min. Serum samples were diluted to 1:100 with PBS containing 1% BSA and 0.05% Tween 20, and then applied to the DNA-coated 96-well plates. Serum from a 12-month-old NZB/W F_1 female mouse was used as a control. After washing three times with PBS containing 0.05% of Tween

20, ANAs were detected with anti-mouse IgG conjugated with HRP as detection antibodies. The total IgM and IgG levels were measured with a Mouse IgM ELISA Quantitation Set and a Mouse IgG ELISA Quantitation Set (Bethyl Laboratory, Inc.), respectively, according to the manufacturer's protocols. To titrate anti-DNA antibodies, a positive control serum from an old female NZB/W F_1 mouse was examined for the anti-dsDNA and anti-ssDNA levels using mouse monoclonal anti-dsDNA IgG2a (Abcam, Cambridge, UK), which is also cross-reactive with ssDNA on ELISA.

Flow cytometry

Spleens were isolated from B6 and *RIIB*$^{-/-}$ mice, and suspended as single cells with PBS containing 1% BSA. Red blood cells were depleted by lysis with 0.144 M NH_4Cl. 2.0×10^6 cells per sample were blocked with 25 μg/ml anti-FcγRII/III (2.4G2), incubated for 15 min at 4°C, and then stained with fluorochrome-labeled antibodies. All fluorescent antibodies were used at 1:200 dilution. Data were collected with FACSCalibur and FACSAria, and analyzed using CellQuest and FACSDiva software (Becton Dickinson Ltd.), respectively.

Statistical analysis

Statistical analysis was performed using Microsoft Excel for Mac 2011 software version 14.2.3 (Microsoft Corp., Seattle, WA) or Prism6 software (Graph Pad Software Inc., La Jolla, CA). Data are displayed when appropriate as means ± SD. Data were compared for statistical differences using Student's *t* test with two-tailed analysis, Log-rank test, or Chi-square test, as indicated in each figure legend. *P* values are shown in the relevant figures. $P < 0.05$ was considered as statistically significant.

Results

RIIB$^{-/-}$, *SLAM*^{129}, and *RIIB*$^{-/-}$*SLAM*^{129} lines with the B6 background thrive normally

RIIB$^{-/-}$ and *SLAM*^{129} mice were generated by backcrossing our 12th-backcross (N12) *RIIB*$^{-/-}$ mice [13,16] into the B6 genetic background further to the 28th generation (N28). Analysis of a series of microsatellite markers including *D1Mit15*, *36*, and *113* in the vicinities of the *Fcgr2b* and *SLAM* loci revealed the successful separation of the *RIIB*$^{-/-}$ locus and the *SLAM*^{129} locus during the backcross (Figure 1A; for details, see Additional file 1: Figure S1 and Additional file 1: Table S1). We also obtained a mouse line with the combined loci, N28 *RIIB*$^{-/-}$*SLAM*^{129}, as a control (Figure 1A and Additional file 1: Figure S1). Both the N28 *RIIB*$^{-/-}$ (*RIIB*$^{-/-}$SENDAI) and N18 *SLAM*^{129} mice thrived normally, at least up to 45 weeks after birth, and the *RIIB*$^{-/-}$*SLAM*^{129} mice did as well despite the fact that female *RIIB*$^{-/-}$*SLAM*^{129} mice manifested obvious glomerulonephritis, as judged on histology (Figure 1B, see below), which was consistent with our previous observation for N12 *RIIB*$^{-/-}$ mice [16]. Four (3 females and 1 male) out of six (3 of each gender) *RIIB*$^{-/-}$ mice obtained from a breeder (*RIIB*$^{-/-}$TACONIC) died before 45 weeks of age in our facility, due probably to lupus nephritis [21] (Figure 1B). Mice obtained from another facility (*RIIB*$^{-/-}$TOKYO) [18] thrived like our *RIIB*$^{-/-}$ mice did. It should be stressed that our *RIIB*$^{-/-}$SENDAI line and *RIIB*$^{-/-}$ animals from other sources were derived from a common origin [13], and backcrossed into the B6 background at different facilities. These results indicate that, even under identical environmental conditions, FcγRIIB-deficient mice with 129-derived genetic intervals of different lengths around the *RIIB*$^{-/-}$ locus show different mortalities, raising the possibility of some influence(s) of unidentified genetic factor(s) within the intervals in the B6 genetic background. Also, the separation of the *RIIB*$^{-/-}$ locus from that of autoimmune-prone *SLAM*^{129} as well as extensive shortening of the 129-derived interval (*Nuf2* to *Fcgr4*, Figure 1A) allowed the establishment of N28 *RIIB*$^{-/-}$SENDAI mice with a normal survival rate, which we mainly used in our analysis described below.

RIIB$^{-/-}$ mice produce a small amount of ANAs

To gain an insight into the difference between *RIIB*$^{-/-}$ and *SLAM*^{129} mice, and its relation to autoimmunity, we measured the total IgM and IgG levels in sera from these locus-separated lines and the combined line, *RIIB*$^{-/-}$*SLAM*^{129}, as a control, at the age of 24–28 weeks. We found that the IgM levels in *RIIB*$^{-/-}$*SLAM*^{129} mice but not *RIIB*$^{-/-}$ or *SLAM*^{129} mice were higher than that in B6 mice, while the IgG levels were higher in female *RIIB*$^{-/-}$ mice and *RIIB*$^{-/-}$*SLAM*^{129} mice of both genders, but not *SLAM*^{129} mice, than that in B6 mice (Figure 2A). Regarding autoantibodies, both *RIIB*$^{-/-}$ and *SLAM*^{129} mice at 36 weeks of age produced a detectable level of ANAs, but in much smaller amounts than *RIIB*$^{-/-}$*SLAM*^{129} mice did, as shown on immunofluorescent staining of HEp-2 cells combined with ELISA, and the levels were less than one-tenth to that in a 12-month-old NZB/W F_1 positive control mouse (Figure 2B, *upper*). There was a tendency that the ANA production and/or accumulation was more pronounced in female than male *RIIB*$^{-/-}$ mice ($P = 0.067$; Figure 2B, *upper*), the female bias being more evident on the titration with HEp-2-HEPANA Test at 24 weeks of age ($P < 0.0001$; Figure 2B, *lower*). This gender bias was not clear in *SLAM*^{129} mice or a breeder's *RIIB*$^{-/-}$ line (Figure 2B). We also checked the IgG subclass of ANAs by HEp-2 ELISA (Figure 2C), and found that IgG2c was the most prominently produced subclass of ANAs in *RIIB*$^{-/-}$ mice, suggesting that type 1 helper T cells are dominantly activated.

Examination of the staining profile of HEp-2 cells (Figure 3A, B) indicated that ANAs detected in sera

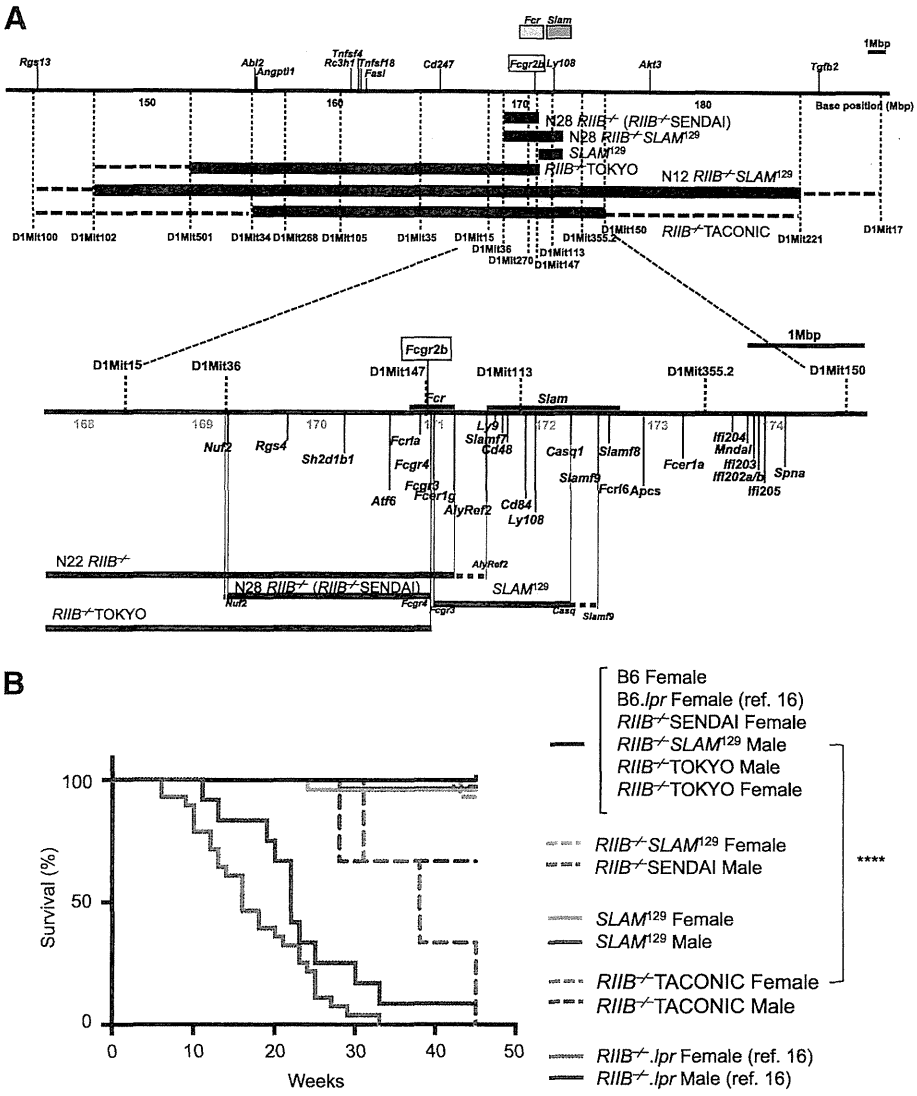

Figure 1 Chromosomal configurations in the vicinity of the *Fcgr2b* gene and *SLAM* locus of congenic mouse lines. (A) Physical mapping was compiled according to the Ensemble Genome Browser (http://www.ensembl.org/). *Upper*, gross schematic view, and *Lower*, detailed genomic structure with SSLP markers, and the genes related to the immune system and examined by SNP analysis (Additional file 1: Table S1 and Additional file 1: Figure S1). Scale bar =1 Mbp. Thick horizontal bars below the map indicate 129 strain-derived intervals, and the flanking, thin broken lines denote intervals unidentified for the B6 or 129 strain. Other areas not shown were derived from B6. The *RIIB*$^{-/-}$TACONIC line had a 129-derived interval from *D1Mit34* to *D1Mit150* at the minimum, while our N12 *RIIB*$^{-/-}$ had an interval from *D1Mit102* to *D1Mit221* at the minimum, according to our analysis. The *Fcr* and *SLAM* loci are shown as shaded boxes at the top of the *Upper* panel or as thick lines above the map in the *Lower* panel. The *Fcgr2b* gene is boxed. When pertinent, we refer to our N28 *RIIB*$^{-/-}$ mice used in the present study as *RIIB*$^{-/-}$SENDAI and those obtained or purchased from others as *RIIB*$^{-/-}$TOKYO or *RIIB*$^{-/-}$TACONIC, respectively, in order to distinguish the data in figures. **(B)** Survival curves for B6 (female, *n* =17), *RIIB*$^{-/-}$SENDAI (female, *n* =30; male, *n* =35), *SLAM*^{129} (female, *n* =23; male, *n* =27), *RIIB*$^{-/-}$*SLAM*^{129} (female, *n* =14; male, *n* =18), *RIIB*$^{-/-}$TOKYO (female, *n* =7; male, *n* =4), and *RIIB*$^{-/-}$TACONIC (female, *n* =3; male, *n* =3) mice. Mice of different lines were examined as to their survival until week 45. For comparison, survival curves for B6.*lpr* (female, *n* =17) and *RIIB*$^{-/-}$*lpr* (female, *n* =28; male, *n* =12) from our previous study [16] are superimposed. ****Significantly different between female *RIIB*$^{-/-}$TACONIC *vs* female *RIIB*$^{-/-}$SENDAI (*P* <0.0001, Log-rank test).

from female *RIIB*$^{-/-}$ mice at 24 weeks of age comprised a mixture of anti-DNA, histone and nucleolus antibodies, and others, because the staining could be classified into nucleolar, homogeneous, and other types, while for the ANAs at 28 and 36 weeks of age peripheral-type staining was dominant, indicating the anti-dsDNA antibodies were major (Figure 3C). When we compared the staining profiles in female *RIIB*$^{-/-}$ and *SLAM*^{129} mice at 24 weeks of age, we observed that the peripheral-type staining was dominant in *SLAM*^{129} mice (Figure 3C, *lower*), suggesting that the compositions of ANAs produced by *RIIB*$^{-/-}$ and *SLAM*^{129} mice

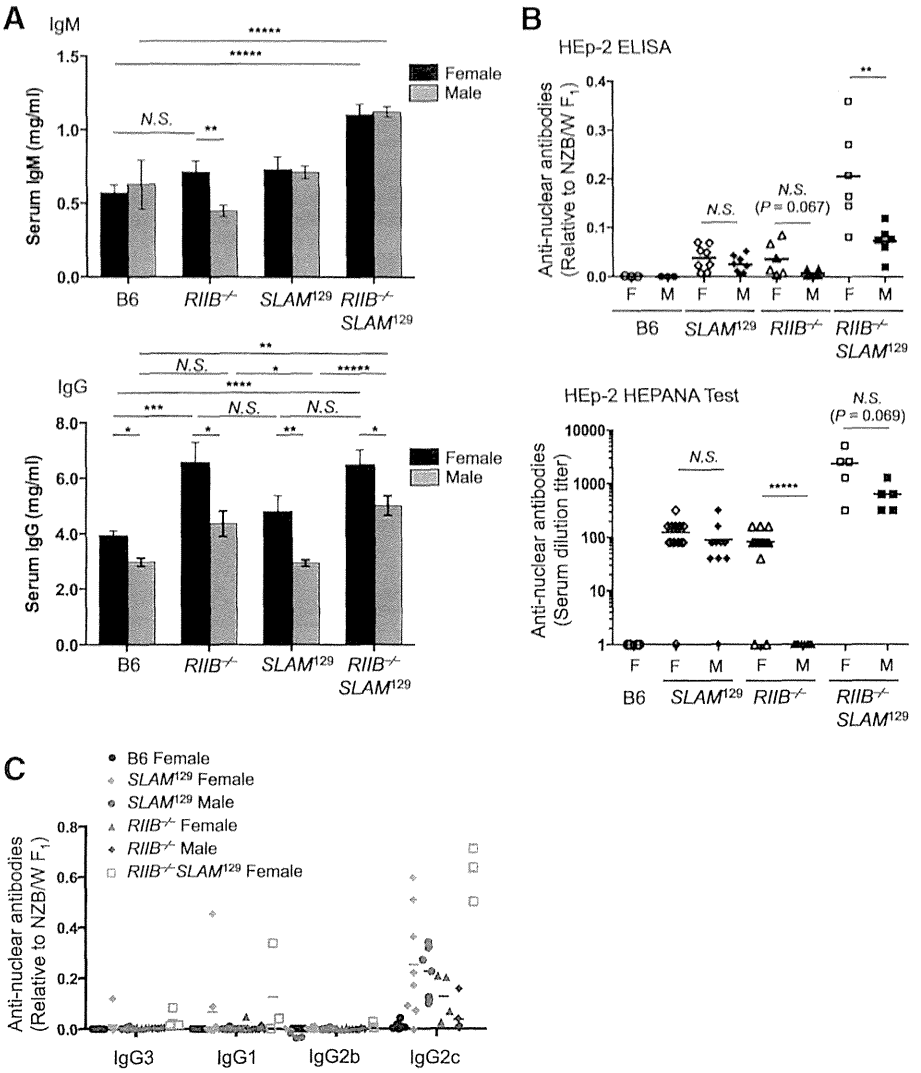

Figure 2 Female-biased production of anti-nuclear antibodies in *RIIB*$^{-/-}$ mice. (A) The total IgM and IgG levels in sera from different lines, including B6, *RIIB*$^{-/-}$, *SLAM*^{129}, and *RIIB*$^{-/-}$*SLAM*^{129}, at 24–28 weeks of age of both genders were measured by ELISA. For IgM and IgG determinations in male B6 mice, n =3 and 5, respectively; for other determinations, $n \geq 8$. The data in each panel are from two separate measurements and are presented as means ± S.D. *P <0.05; **P <0.01; ***P <0.001; ****P <0.0001; *N.S.*, not significant. Student's t-test. **(B)** Spontaneous production of ANAs by *SLAM*^{129} (n =16), *RIIB*$^{-/-}$ (n =12), *RIIB*$^{-/-}$*SLAM*^{129} (n =12), and B6 (n =6) mice at 36 weeks (*Upper*) or 24 weeks (*Lower*) of age of both genders was measured in serum samples by HEp-2 staining combined with ELISA (*Upper*) and HEp-2-HEPANA Test (*Lower*), and expressed as the levels relative to that in sera collected from a 12-month-old female NZB/W F_1 mouse, whose anti-dsDNA and anti-ssDNA levels were 6.64 μg/ml and 4.69 μg/ml, respectively. Horizontal lines represent the mean values. **P <0.01; ****P <0.0001; *N.S.*, not significant. Student's t-test. **(C)** IgG isotypes of ANAs in sera from *RIIB*$^{-/-}$ and *SLAM*^{129} mice of both genders. ANA IgG isotypes were determined by HEp-2 staining combined with ELISA, and presented as values relative to that in a 12-month-old NZB/W F_1 control female mouse, as described in B.

at 24 weeks of age are qualitatively different, as determined based on the HEp-2 cell staining profiles, albeit the assay used is not sufficiently quantitative.

In addition to determination of the total ANA levels described above, we also measured the anti-DNA levels in sera from mice at different ages by ELISA. Anti-single-stranded (ss)DNA and -double-stranded (ds)DNA antibodies were detected, albeit in very small amounts, in *RIIB*$^{-/-}$ mice at around 12 weeks and 16–20 weeks of age, respectively, and the levels were higher in females than males after 28 weeks of age, while B6 female mice, as healthy controls, at the same ages did not significantly produce anti-DNA antibodies as compared to those in a NZB/W F_1 mouse as a disease control (Figure 4A). As was the case for the serum ANA levels, *RIIB*$^{-/-}$*SLAM*^{129} mice produced anti-DNA antibodies, particularly abundantly in females (Figure 4B). The bias was not clear in a breeder's *RIIB*$^{-/-}$ line (Figure 4C, D). These results

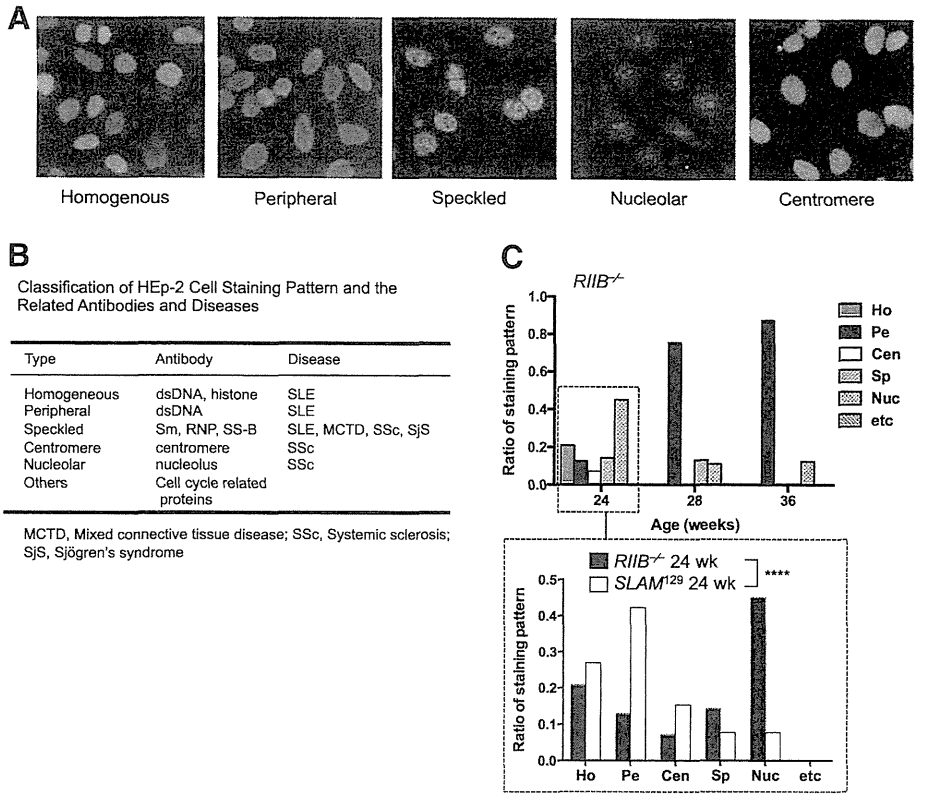

Figure 3 Qualitative analysis of ANAs in *RIIB*$^{-/-}$ and *SLAM*^{129} mice. (A) Classification of staining profiles of HEp-2 cells. Representative staining patterns observed for serum samples from *RIIB*$^{-/-}$*SLAM*^{129} mice are shown as fluorescently stained cells. **(B)** The classification of HEp-2 cell staining pattern and the related antibodies and diseases. **(C,** *Upper*) Comparison of the HEp-2 staining patterns of female *RIIB*$^{-/-}$ mice at different ages. The staining patterns were divided into six categories as shown in **(B)**. **(C,** *Lower*) Comparison of the staining patterns between female *RIIB*$^{-/-}$ and *SLAM*^{129} mice at 24 weeks of age. For classification, staining profiles in sera from ≥13 mice were evaluated. Ho, homogeneous; Pe, peripheral; Cen, centromere; Sp, speckled; Nuc, nucleolar; etc, others. Significantly different between *RIIB*$^{-/-}$ and *SLAM*^{129} (P <0.0001 by Chi-square test).

indicate that our *RIIB*$^{-/-}$ and *SLAM*^{129} mice differently produce and/or maintain ANAs including anti-DNA autoantibodies.

Weak glomerulonephritis in *RIIB*$^{-/-}$ mice

Given the production of anti-DNA antibodies by *RIIB*$^{-/-}$ mice, we next examined the renal histology, and scored the glomerulonephritis in male and female *RIIB*$^{-/-}$, *SLAM*^{129}, and *RIIB*$^{-/-}$*SLAM*^{129} mice at 36 weeks of age (Figure 5). While control female *RIIB*$^{-/-}$*SLAM*^{129} mice exhibited severe glomerulonephritis with occasional crescent formation, mesangial cell proliferation, macrophage and neutrophil infiltration, and lobulation of glomeruli, female *RIIB*$^{-/-}$ mice exhibited weak but less severe glomerulonephritis than control *RIIB*$^{-/-}$*SLAM*^{129} animals, with mesangial cell proliferation and neutrophil infiltration (Figure 5A, B). Male *RIIB*$^{-/-}$, and male and female *SLAM*^{129} mice only showed occasional mesangial cell proliferation. We also examined IgG-IC deposition in renal samples by immunofluorescence microscopy, and found that only female *RIIB*$^{-/-}$ and *RIIB*$^{-/-}$*SLAM*^{129} mice exhibited weak deposition (Figure 5C, D), but female *SLAM*^{129} mice did not (Figure 5C). These results indicate that the development of glomerulonephritis observed in *RIIB*$^{-/-}$ mice had occurred in a female-biased manner, while *SLAM*^{129} mice did not develop the disease at least until 36 weeks of age. It is noteworthy that the development of glomerulonephritis seemingly correlated with the female-biased ANA increase in *RIIB*$^{-/-}$ and *RIIB*$^{-/-}$*SLAM*^{129} animals described above (Figure 4A–C), but *SLAM*^{129} mice did not manifest the disease regardless of the fact that they produced ANAs at comparable levels to female *RIIB*$^{-/-}$ mice, at least at 24 weeks of age (Figure 2B, C). This notion suggests a contribution of FcγRIIB to protection from IgG-IC deposition in glomeruli and glomerulonephritis.

Splenic germinal center formation was grossly normal in *RIIB*$^{-/-}$ mice

We were interested in determining why ANAs and anti-DNA antibodies in sera were increased in *RIIB*$^{-/-}$ mice, albeit in very small amounts. To this end, we isolated spleens, and examined their weights, histology, and cellularity. While splenomegaly was

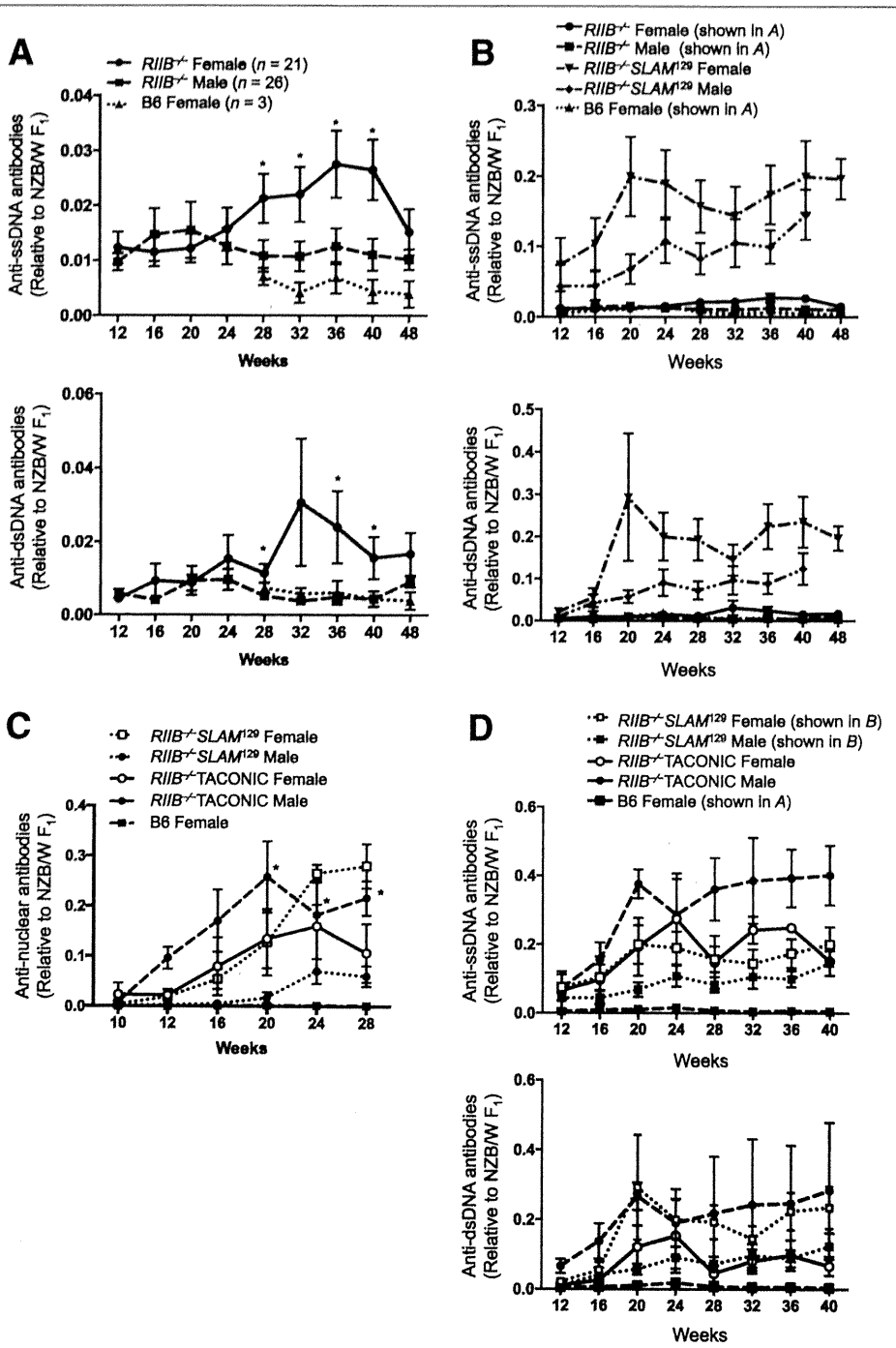

Figure 4 Increase of anti-DNA antibodies in *RIIB*$^{-/-}$ mice. (A) Anti-ssDNA (*upper*) and -dsDNA (*lower*) antibody levels in sera from female and male *RIIB*$^{-/-}$ mice, and female B6 mice at different ages. Anti-DNA levels were measured by ELISA and presented as values relative to that in a 12-month-old NZB/W F_1 control female mouse, whose anti-dsDNA and anti-ssDNA levels were 6.64 μg/ml and 4.69 μg/ml, respectively. Each data point represents the mean value ± SD ($n \geq 3$). Significantly different between female *RIIB*$^{-/-}$ and B6 (*P <0.05) with Student's t-test. **(B–D)** Anti-DNA antibody **(B, D)** levels and ANA levels **(C)** in sera from female and male *RIIB*$^{-/-}$SENDAI or TACONIC mice, *RIIB*$^{-/-}$*SLAM*^{129}, and B6 mice at different ages. Anti-DNA levels and ANAs were measured by ELISA and HEp-2 staining combined with ELISA, respectively, and presented as values relative to that in a 12-month-old NZB/W F_1 control female mouse as described in A. Each data point represents the mean value ± SD ($n \geq 3$). *P <0.05. Student's t-test. In **B**, the plots for *RIIB*$^{-/-}$ and B6 mice in **A** were superimposed for comparison. In **D**, the plots for *RIIB*$^{-/-}$*SLAM*^{129} and B6 mice in **B** and **A**, respectively, were superimposed for comparison.

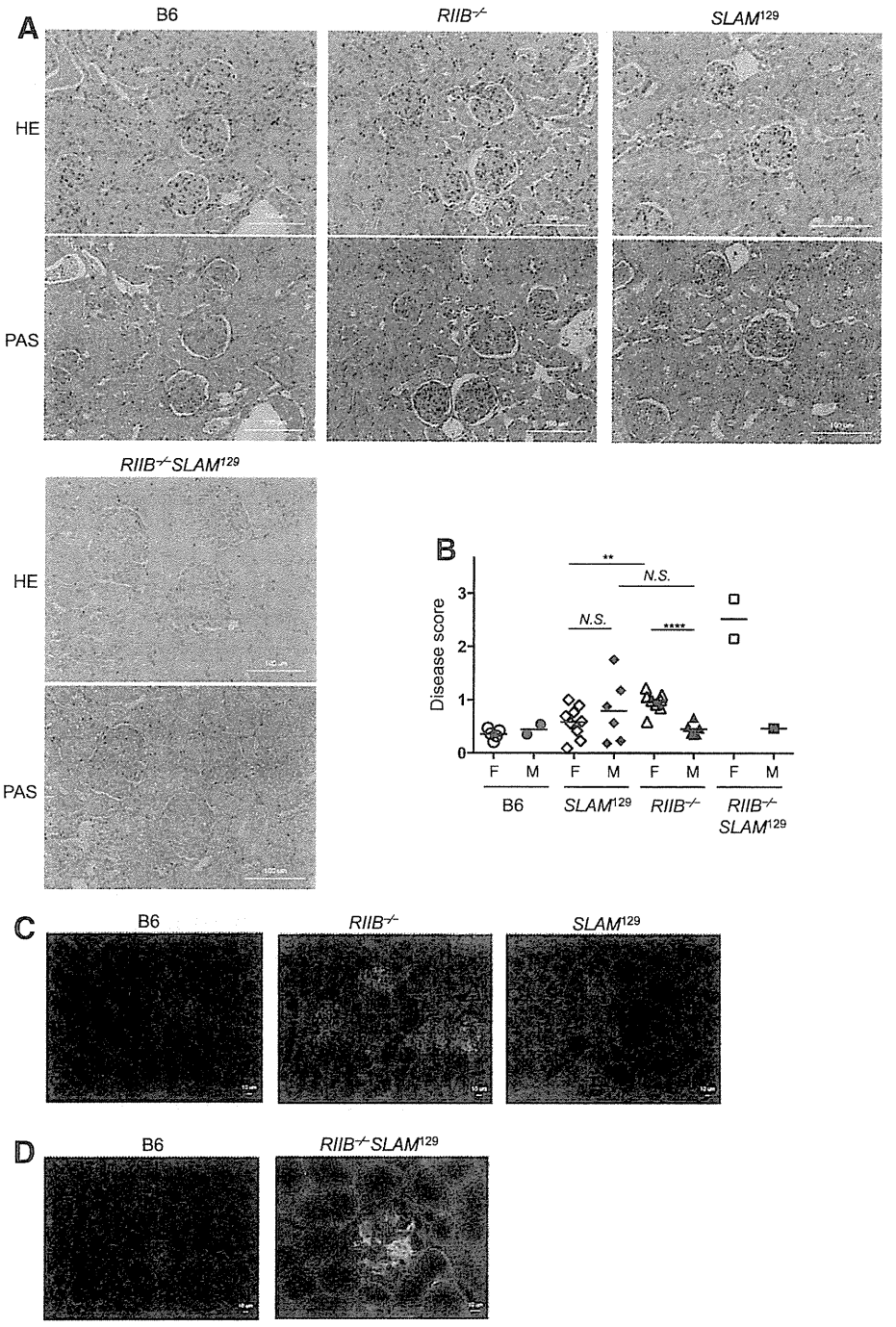

Figure 5 Glomerulonephritis in *RIIB*$^{-/-}$, *SLAM*^{129}, and *RIIB*$^{-/-}$*SLAM*^{129} mice. (A) Kidney sections from each mouse line at week 45 were stained with HE (*upper*) and PAS (*lower*) for examination of glomerular disease, which was assessed according to the criteria depicted in *Methods*. Original magnification, ×200. Scale bar, 100 μm. **(B)** Comparison of the disease scores among *RIIB*$^{-/-}$, *SLAM*^{129}, *RIIB*$^{-/-}$*SLAM*^{129} and B6 mice at 45 weeks of age. *F*, female; *M*, male. Horizontal bars denote the mean values, excepting the plot of *RIIB*$^{-/-}$*SLAM*^{129} male for single determination. ***P <0.001 (n =3–6). For scoring, ≥25 glomeruli were examined for each line. Student's *t*-test. **(C, D)** For IgG-immune complexes (IgG-ICs) deposition, kidney sections from each mouse line at week 45 were stained with FITC-anti mouse IgG. Original magnification, ×200 **(C)** or × 100 **(D)**. Scale bar, 10 μm. The figure is representative of most of the glomeruli observed in three mice per group.

observed in *RIIB*$^{-/-}$*SLAM*^{129} mice, it was much less evident in *RIIB*$^{-/-}$ mice (Figure 6A, *left*). This was, however, not pronounced in the total splenic lymphocytes of *RIIB*$^{-/-}$ animals (Figure 6A, *right*). Immunohistochemistry of spleen sections prepared from naïve mice indicated that germinal center (GC) formation was grossly